JACS Au
AN OPEN ACCESS JOURNAL OF THE AMERICAN CHEMICAL SOCIETY

pubs.acs.org/jacsau
Article

Structure-Based High-Efficiency Homogeneous Antibody Platform by Endoglycosidase Sz Provides Insights into Its Transglycosylation Mechanism

Published as part of JACS Au virtual special issue "Biocatalysis in Asia and Pacific".

Yin-Cheng Hsieh,[#] Hong-Hsiang Guan,[#] Chien-Chih Lin, Teng-Yi Huang, Phimonphan Chuankhayan, Nai-Chi Chen, Nan-Hsuan Wang, Pu-Ling Hu, Yi-Chien Tsai, Yen-Chieh Huang, Masato Yoshimura, Pei-Ju Lin, Yih-Huang Hsieh,* and Chun-Jung Chen*

Cite This: *JACS Au* 2024, 4, 2130−2150
Read Online

ACCESS | Metrics & More | Article Recommendations | Supporting Information

ABSTRACT: Monoclonal antibodies (mAbs) have gradually dominated the drug markets for various diseases. Improvement of the therapeutic activities of mAbs has become a critical issue in the pharmaceutical industry. A novel endo-*β*-*N*-acetylglucosaminidase, EndoSz, from *Streptococcus equisubsp. zooepidemicus Sz105* is discovered and applied to enhance the activities of mAbs. Our studies demonstrate that the mutant EndoSz-D234M possesses an excellent transglycosylation activity to generate diverse glycoconjugates on mAbs. We prove that EndoSz-D234M can be applied to various marketed therapeutic antibodies and those in development for antibody remodeling. The remodeled homogeneous antibodies (mAb-G2S2) produced by EndoSz-D234M increase the relative ADCC activities by 3−26-fold. We further report the high-resolution crystal structures of EndoSz-D234M in the *apo*-form at 2.15 Å and the complex form with a bound G2S2-oxazoline intermediate at 2.25 Å. A novel pH-jump method was utilized to obtain the complex structure with a high resolution. The detailed interactions of EndoSz-D234M and the carried G2S2-oxazoline are hence delineated. The oxazoline sits in a hole, named the oxa-hole, which stabilizes the G2S2-oxazoline in transit and catalyzes the further transglycosylation reaction while targeting Asn-GlcNAc (+1) of Fc. In the oxa-hole, the H-bonding network involved with oxazoline dominates the transglycosylation activity. A mobile loop2 (a.a. 152−159) of EndoSz-D234M reshapes the binding grooves for the accommodation of G2S2-oxazoline upon binding, at which Trp154 forms a hydrogen bond with Man (−2). The long loop4 (a.a. 236−248) followed by helix3 is capable of dominating the substrate selectivity of EndoSz-D234M. In addition, the stepwise transglycosylation behavior of EndoSz-D234M is elucidated. Based on the high-resolution structures of the *apo*-form and the bound form with G2S2-oxazoline as well as a systematic mutagenesis study of the relative transglycosylation activity, the transglycosylation mechanism of EndoSz-D234M is revealed.

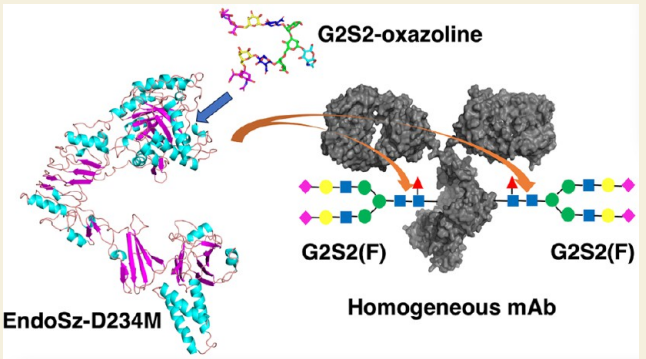

KEYWORDS: *endo-β-N-acetylglucosaminidase, EndoSz, N-glycan, G2S2-oxazoline, transglycosylation, homogeneous antibody platform*

INTRODUCTION

Therapeutic monoclonal antibodies (mAbs) have become increasingly important in the pharmaceutical industry.[1,2] In 2021, four of the top ten best-selling drugs worldwide were mAbs, among which two were COVID-19 vaccines.[3] mAb treatments encompassed many diseases, including cancers, autoimmune, and infectious diseases.[4−6] For cancer therapy, mAb treatments recognize particular biomarkers on the tumor cell surface and enhance cell apoptosis with different mechanisms, such as antibody-dependent cellular cytotoxicity (ADCC), complement-dependent cytotoxicity (CDC), antibody-dependent cellular phagocytosis (ADCP), and blockade of signal pathways. Compared with small-molecule drugs, mAbs are more target-specific with lower side effects on the patients.

Two Fab domains of mAbs contain a variable complementarity-determining region (CDR) for antigen recognition. One Fc domain with *N*-glycans mediates effector functions, including ADCC, ADCP, vaccinal effect, CDC, etc., through

Received: January 2, 2024
Revised: March 29, 2024
Accepted: March 29, 2024
Published: April 11, 2024

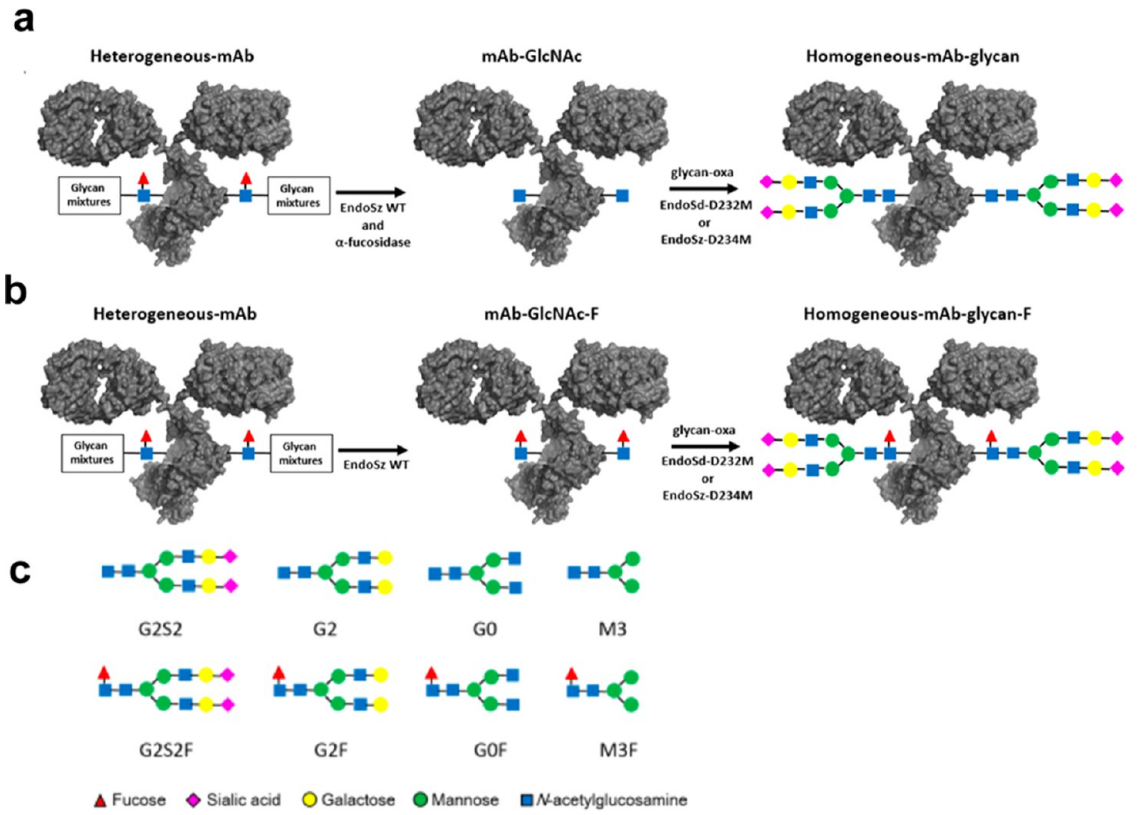

Figure 1. Overall process of the homogeneous mAbs platform. The production processes of homogeneous glycans (a) without fucose (F) and (b) with fucose are performed in the homogeneous platform. The cell-expressed mAbs with heterogeneous glycan mixtures were removed by wild-type EndoSz with or without α-fucosidase to generate mAb-GlcNAc or mAb-GlcNAc-F. Subsequently, EnodSd-D232M or EnodSz-D234M was used to conjugate glycan-oxazoline and produce homogeneous mAbs with fucose or without fucose. (c) The cartoon diagrams of biantennary glycans (M3; $Man_3GlcNAc_2$, G0; $GlcNAc_2Man_3GlcNAc_2$, G2; $Gal_2GlcNAc_2Man_3GlcNAc_2$, G2S2; $Sia_2Gal_2GlcNAc_2Man_3GlcNAc_2$) with and without fucose are proven to be able to work in the platform. The glycan-oxa stands for glycan-oxazoline.

interacting with Fc receptors on immune cells, such as FcγRIIIa, FcγRIIa, FcγRIIIb, FcγRIIb, and the complement factor C1q.[7−10] The Fc domain contains a conserved *N*-glycosylation site, namely, Asn297, attached with heterogeneous glycan types, such as biantennary (M3, G0F, G1F, G2F, G0, G1, and G2 complex types) (Figure 1) and triantennary glycans (high-mannose and hybrid types) in various expression systems. The core fucose moiety of Fc glycan could hamper the carbohydrate−carbohydrate interactions between Fc and FcγRIIIa, resulting in a decrease of the binding constant by ∼100-fold[11] and reducing the cell-killing efficiency. The Chinese hamster ovary (CHO) cell expression generally produces glycan-containing mAbs in the forms of G0F, G1F, and G2F with fucose moieties, which reduce ADCC. The removal of Fc glycan resulted in a loss of ADCC.[12] Thus, mAb cytotoxicity is suggested to be effectively controlled by the composition of *N*-glycans on the Fc region. Although modified CHO cells with FUT8 (α-1,6-fucosyltransferase 8) gene knockout[13,14] or upregulation of bisecting GlcNAc (*N*-acetylglycosamine) transferase GnT-III[15] were reported to reduce the glycan complexity of mAbs, the development of better or more general methods to control the *N*-glycans on mAbs is still of great interest.

N-Acetylglucosaminidases (NAGs), belonging to the glycoside hydrolase family 18 (GH18) with a conserved catalytic motif DxxDxDxE, comprise four groups: Groups (I) and (II) both chitinolytic NAGs, (III) *N*-glycan processing NAGs, and (IV) hexosaminidases, based on phylogenetic analysis.[16] Endo-β-*N*-acetylglucosaminidases (EC 3.2.1.96) (ENGases), NAGs of Group III, hydrolyze the β-1,4 glycosidic bond between the first two *N*-acetylglucosamine moieties in *N*-linked sugar chains of glycoproteins.[17,18] ENGases also possess a weak transglycosylation activity to synthesize the specific glycan on the first *N*-acetylglucosamine moiety linked to Asn.[19−21] Its dual hydrolysis/transglycosylation ability is extensively utilized in the glycoengineering of therapeutic proteins or antibodies to remodel glycoproteins for specific homogeneous *N*-glycans.[22] This is especially true for therapeutic monoclonal antibodies IgGs due to the composition and homogeneity of two *N*-glycans attached to the Asn297 of IgG-Fc regions that can affect ADCC and CDC.[23,24] The glycoforms on IgGs are hence critical for their efficacy. EndoS and EndoS2 are substrate-specific ENGases for IgGs.[25,26]

Enzymatic modification of the Fc region is a solution to establish homogeneous mAbs to enhance ADCC. Chemoenzymatic remodeling could be achieved by removing the glycan mixture and conjugating homogeneous glycans.[27] Several ENGases that can remove the glycan mixture on mAbs have been reported. For instance, Endo-D,[28] Endo H,[29] EndoLL,[12] and Endo-M[30] can hydrolyze glycans with high-mannose or terminal mannose types. EndoS[25] and EndoSd[31] hydrolyze nonfucosylated and fucosylated complex-type *N*-glycans on the Fc domain, but not high-mannose types. On the other hand, glycosynthases for the antibody Fc have been reported. Endo-D-N322Q[32] and Endo-M-N175Q[33] can only transfer the short-chain complex-type *N*-glycan to Fc, whereas

https://doi.org/10.1021/jacsau.4c00004
JACS Au 2024, 4, 2130−2150

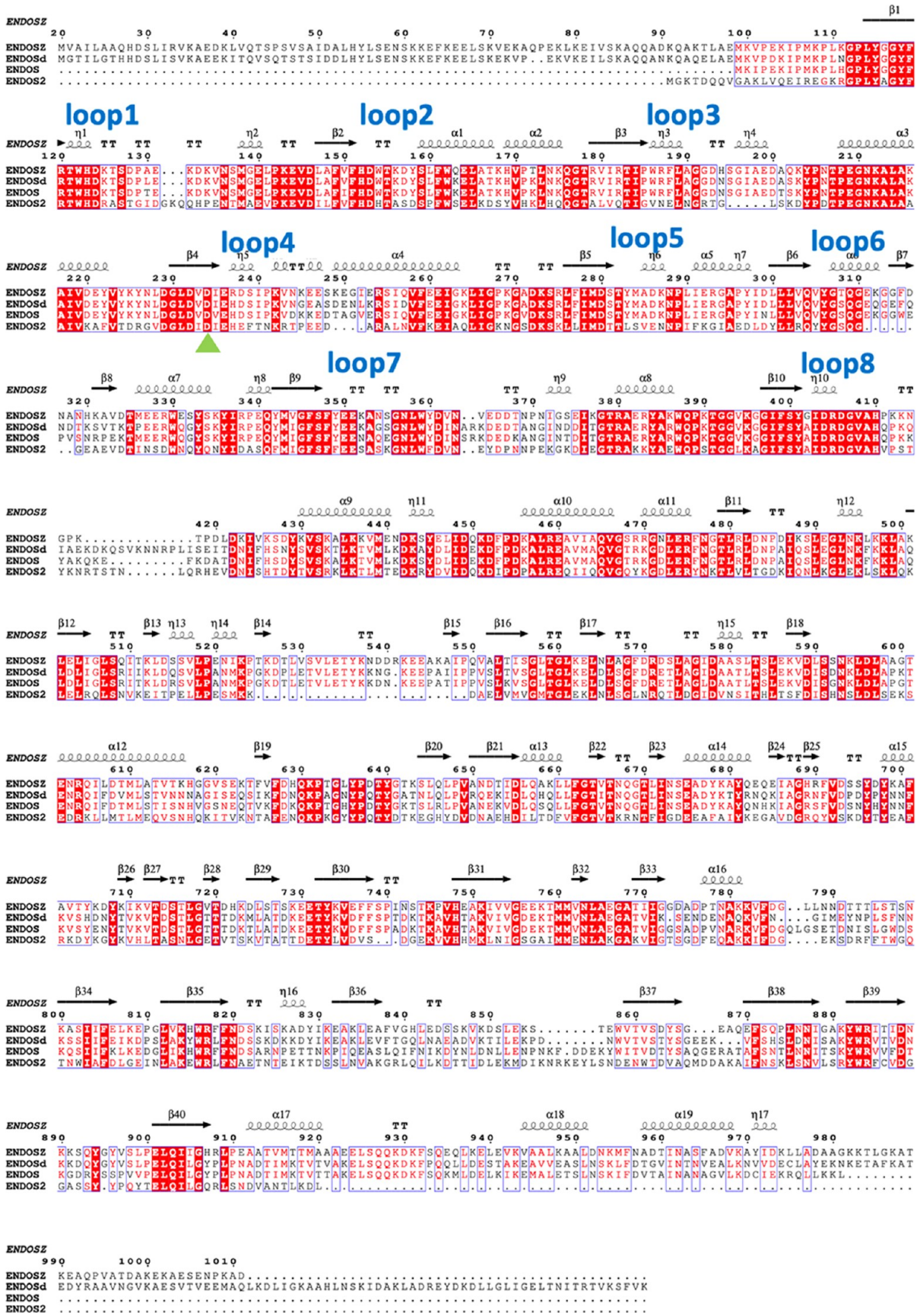

Figure 2. Sequence alignment of EndoSz, EndoSd, EndoS, and EndoS2. The loops of EndoSz surrounding the active site are labeled in light blue. The mutation sites, D234 of EndoSz and D232 of EndoSd, are marked with the green triangle.

https://doi.org/10.1021/jacsau.4c00004
JACS Au 2024, 4, 2130−2150

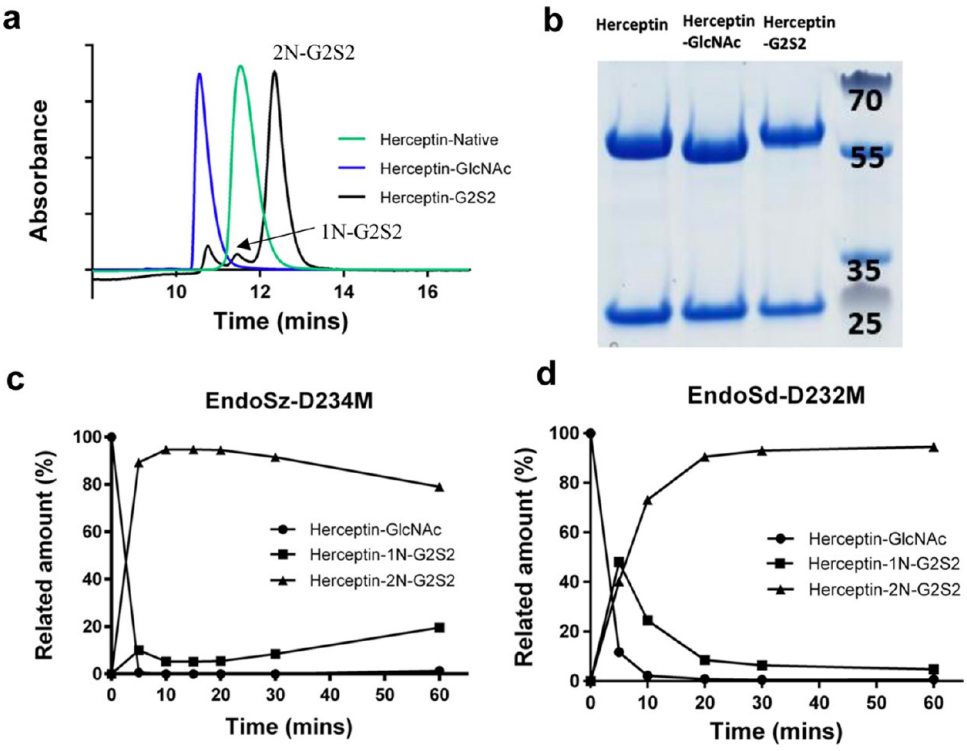

Figure 3. Detection methods and time-dependent transglycosylation analysis for the homogeneous mAbs platform (demonstrated by EndoSz-D234M). (a) HPLC-based glycan analysis (HBGA) method. Original Herceptin (green) had a retention time of 11.45 min, and Herceptin-GlcNAc (blue) shifted to 10.55 min. In the transglycosylation of G2S2-oxazoline, the profile of Herceptin-G2S2 (black) can be clearly distinguished by 1N-G2S2 (hemiglycosylated) and 2N-G2S2 (fully glycosylated) with retention times of 11.53 and 12.35 min, respectively. In the transglycosylation process, the peaks sequentially shifted from Herceptin-GlcNAc to Herceptin-1N-G2S2 and Herceptin-2N-G2S2, which allowed us to monitor the process. (b) SDS-PAGE result for comparison. Herceptin-1N-G2S2 and Herceptin-2N-G2S2 cannot be distinguished in the lane (Herceptin-G2S2). (c) Transglycosylation reactions with the molar ratio of 20:1 (G2S2-oxazoline and Herceptin-GlcNAc) by EndoSz-D234M and (d) with a higher molar ratio of 150:1 by EndoSd-D232M. Both reactions started with 100% Herceptin-GlcNAc. The time-dependent transglycosylation results for the remaining Herceptin-GlcNAc, produced Herceptin-1N-G2S2, and Herceptin-2N-G2S2 were recorded.

Endo-F3-D165Q[34] can only transfer the glycan to the fucosylated Fc domain. EndoS-D233Q[27] can conjugate various biantennary complex types, whereas EndoS2-D184 M[35] can accept wild substrates, including complex (CT), high-mannose (HM), and hybrid (Hy) types.

To understand the mechanism of chemoenzymatic re-engineering, structures of the enzymes complexed with glycans are needed. To date, several crystal structures of ENGases have been reported: (1) HM-type-specific ENGases, including Endo-A,[36] Endo-F,[37] Endo H,[38] Endo T,[39] and EndoBT (PDB entry 3POH); (2) Endo-F3[40] and EndoS,[41,42] belonging to CT-type-specific ENGases, and EndoS2, with a broader hydrolysis activity toward HM, Hy, and CT glycans,[43,44] in complex only with G2 products; (3) *holo*-form Endo-CoM,[45] a core-fucosylated-type-specific ENGase; and (4) EndoBT-3987 from *Bacteroides thetaiotaomicron* in complex with the HM-type substrate and the product.[46]

In this work, we report two mutant enzymes of EndoSd from *Streptococcus dysgalactiae* subsp. *dysgalactiae* (ANI26082.1) and EndoSz with glycosynthase activity. The D234M mutant of EndoSz, namely, EndoSz-D234M, a novel ENGase, possesses great glycosynthase activity to synthesize homogeneous biantennary CT-type glycans on antibody IgG and can be utilized in the homogeneous *N*-glycan platform in the pharmaceutical industry. We demonstrate the excellent homogeneous *N*-glycan conjugation results of OBI-888, Herceptin, Perjeta, Erbitux, Rituxan, OBI-898, Vectibix, Humira, Keytruda, and Bavencio with EndoSz-D234M. The ADCC of homogeneous mAbs in related cell systems increases 3−26 times compared to heterogeneous mAbs. To understand the synthesis mechanism of EndoSz-D234M, we determine crystal structures of EndoSz-D234M in an *apo*-form and a complex form with G2S2-oxazoline at high resolution. Detailed interactions between EndoSz-D234M and G2S2-oxazoline are delineated. A structural comparison of *apo*-EndoSz and its complex (EndoSz/G2S2-oxazoline) highlights the conformational alternations related to the carbohydrate binding and involvement in substrate selectivity. The time-dependent transglycosylation activity together with the docking complex structure of EndoSz-D234M/IgG-Fc elucidates the stepwise transglycosylation process of EndoSz-D234M. Conclusively, the transglycosylation mechanism of EndoSz-D234M is revealed.

RESULTS AND DISCUSSION

EndoSz, a Novel ENGase, Applied in the Homogeneous Antibody Platform

In the biopharmaceutical industry, antibodies produced by CHO cells always contain heterogeneous glycans on the Asn297 position of Fc. Enzymatic modification is an advanced and developing method to generate mAbs with homogeneous *N*-glycans for the enhancement of mAb activities. The enzymatic cleavage of glycan and transglycosylation are essential steps in the *N*-glycan-homogeneous process. For glycan cleavage, a previous study showed that EndoSd well-

https://doi.org/10.1021/jacsau.4c00004
JACS Au 2024, 4, 2130−2150

hydrolyzed biantennary glycans.[31] To search for a better new ENGase utilized in homogeneous antibody re-engineering in the pharmaceutical industry, we performed a BLAST search of protein sequences with the reference sequence of EndoS. We discovered EndoSz, a novel ENGase from *Streptococcus equi subsp. zooepidemicus Sz105* (KIS14581.1), comprising 992 amino acids with a molecular mass of ∼110 kDa, in addition to EndoSd.

We used human and bovine IgGs as substrates to examine the glycan-cleavage ability of EndoSz (Figure S1). In addition, the native Herceptin IgG can also be hydrolyzed by EndoSz, and the remaining *N*-glycans on Herceptin IgG were recorded (Figure S2). The results demonstrated that EndoSz can primarily hydrolyze the biantennary complex-type *N*-glycan. Herceptin, with only one *N*-acetylglucosamine (Herceptin-GlcNAc) on N297, was generated (>99%) after the treatment of EndoSz and α-fucosidase enzymes. The results indicated that EndoSz exhibits deglycosylation specificity toward complex-type biantennary glycans. In addition, we have demonstrated that EndoSz-D234M exhibits specificities toward M3, M2F, G0, G0F, G2, G2F, G2S2, and G2S2F in transglycosylation activities (Figure 1). We, then, set up the homogeneous *N*-glycan platform incorporating EndoSz, EndoSd, or each mutant, separately, for the production of homogeneous mAbs with or without fucose (Figure 1). Moreover, for the removal of plausible high-mannose glycan on Fab, we sequentially applied additional enzymes, Endo H or Endo-M,[29,30] in the cleavage step for the complete removal of glycans on Fab in the platform. With this platform, the therapeutic mAbs with the desired homogeneous *N*-glycans can be produced effectively.

Several ENGases, such as Endo-F3, EndoS, and EndoS2, are known for their specificities toward IgG-Fc.[27,34,35] In terms of transglycosylation activity, EndoS2 mutants target three major glycan types: high-mannose, hybrid, and complex types.[35,47] Interestingly, Endo-F3 mutants can use both bi- and triantennary complex-type *N*-glycans as transglycosylation substrates.[34] Notably, both EndoSz and EndoS are highly specific, showing a distinctive preference for biantennary complex-type *N*-glycans. This unique specificity distinguishes them from other ENGases. Despite their similar specificity, the EndoSz mutant demonstrates superior performance compared to EndoS, as described later.

Transglycosylation Investigation of EndoSz-D234M and EndoSd-D232M

Transglycosylation, the most important step in the pharmaceutical homogeneous *N*-glycan platform, determines the quality of homogeneous mAbs. EndoS2 employed with D184M mutation has previously been reported to have a high transglycosylation activity,[27] First, we generated EndoSz-D234M and EndoSd-D232M mutants for the transglycosylation investigation based on multiple-sequence analyses (Figure 2). The established HPLC-based glycan analysis (HBGA) method with an amide column was utilized to precisely monitor the transglycosylation process. The retention time of native Herceptin was shown at 11.45 min (Figure 3a). After the glycan cleavage by EndoSz-WT and α-fucosidase, the retention time of Herceptin with one GlcNAc (Herceptin-GlcNAc) shifted from 11.45 to 10.55 min with the molecular mass 145 573.2 Da with intact mass and sodium dodecyl-sulfate polyacrylamide gel electrophoresis (SDS-PAGE) analyses (Figure 3b). It is interesting to note that HBGA can identify the hemiglycosylated Herceptin (Herceptin-1N-G2S2) and fully glycosylated Herceptin (Herceptin-2N-G2S2), which is however difficult to distinguish with SDS-PAGE analysis. In HGBA, Herceptin-1N-G2S2 was found at the retention time of 11.53 min with M_w 147 575.6 Da, whereas Herceptin-2N-G2S2 was found at the retention time of 12.35 min with M_w 149 578.0 Da. Molecular masses were measured with the mass spectrum (Figure S3). We believe that the HBGA method applies to all mAbs systems. The method is employed for further investigations on transglycosylation processes in our platform.

For the transglycosylation process, a high ratio of sugar to antibody would usually generate a higher conjugation efficiency in the transglycosylation step. However, in the pharmaceutical industry, a compromise between the sugar amount and the cost and the control of the process within a reasonable time frame is necessary for optimization of the process. We used Herceptin-GlcNAc and sialylated complex-type *N*-glycan-oxazoline (G2S2-oxazoline) as investigation models to evaluate the transglycosylation activity of EndoSz-D234M and EndoSd-D232M for the expected formation of >90% Herceptin-2N-G2S2 within 60 min.

>90% Herceptin-2N-G2S2 was obtained with EndoSz-D234M with the G2S2-oxazoline/Herceptin molar ratio of 40:1 at 5 min. With a decrease of the G2S2-oxazoline/Herceptin molar ratio to 30:1, >90% Herceptin-2N-G2S2 could be obtained at 10 min. With the G2S2-oxazoline/Herceptin ratio of 20:1, Herceptin-2N-G2S2 reached 89.31% at 5 min, 91.85% at 10 min, and stayed at the same level until 20 min before deglycosylation started (Figure 3c).

With the G2S2-oxazoline/Herceptin ratio decreased to 10:1, 62.61% of Herceptin-2N-G2S2 was obtained at 5 min and 61.48% at 10 min before deglycosylation started; the efficiency with the ratio 10:1 was lower. To optimize the usage of G2S2-oxazoline, the G2S2-oxazoline/Herceptin ratio of 15:1 was utilized, and 80.8% of Herceptin-2N-G2S2 was attained at 5 min before deglycosylation started at 10 min. Therefore, we determined and concluded that the best transglycosylation condition with the EndoSz-D234M enzyme was utilizing the G2S2-oxazoline/antibody ratio of 20:1 with a 20-min reaction time.

The time-dependent HBGA graph (Figure 3c) clearly illustrated that EndoSz-D234M efficiently and quickly bound to Fc and conjugated the glycan (G2S2-oxazoline) at the Asn297 position of Fc with Herceptin-GlcNAc decreased nearly 0%, and about 90% of the fully glycosylated antibody was found. However, the highly efficient transglycosylation enzyme also contributes to the hydrolysis activity. In all trials, deglycosylation occurred while the reaction reached the greatest efficiency of transglycosylation and stayed steady for a period (20 min), which demonstrated the importance of controlling the transglycosylation process time. Notably, during the deglycosylation process (20−60 min), the decrease of Herceptin-2N-G2S2 was accompanied by an increase of Herceptin-1N-G2S2, suggesting the enzyme has a priority in selecting Herceptin-2N-G2S2 as a target rather than Herceptin-1N-G2S2 in the hydrolysis reaction. This phenomenon indicated the importance of the secondary *N*-glycan during the hydrolysis reaction of the first *N*-glycan. The secondary *N*-glycan might facilitate EndoSz-D234M to digest the first *N*-glycan in some unknown manner.

In contrast, the EndoSd-D232M enzyme exhibited inconsistent results with an G2S2-oxazoline/antibody molar ratio of

https://doi.org/10.1021/jacsau.4c00004
JACS Au 2024, 4, 2130−2150

Table 1. Fucosylated Substrate Effect on Transglycosylation Activities with EndoSz-D234M and EndoSd-D232M[a]

enzyme	acceptor	G2S2-oxazoline amount	conjugation		
			GlcNAc(F)	1N-G2S2	2N-G2S2
EndoSz-D234M	Herceptin-GlcNAc	20eq	3.35%	4.80%	91.85%
	Herceptin-GlcNAc-F	20eq	1.72%	4.00%	94.29%
EndoSd-D232M	Herceptin-GlcNAc	150eq	0%	2.11%	97.88%
	Herceptin-GlcNAc-F	150eq	0.71%	4.55%	94.75%

[a]The portions of products GlcNAc(F), 1N-G2S2, and 2N-G2S2 were recorded when the transglycosylation reactions using G2S2 glycans, fucosylated substrates, and nonfucosylated substrates were performed with EndoSz-D234M and EndoSd-D232M, respectively, under the best transglycosylation conditions (G2S2-oxazoline/antibody ratio of 20:1 (20eq) with a 20 min reaction time for EndoSz-D234M; G2S2-oxazoline/antibody ratio of 150:1 (150eq) with a 20 min reaction time for EndoSd-D232M).

20:1 and with 20 min, the best transglycosylation condition of EndoSz-D234M. Only 46.06% Herceptin-2N-G2S2 was generated by EndoSd-D232M, indicating that EndoSz-D234M possesses a glycosynthase activity better than EndoSd-D232M. To obtain a larger amount of fully glycosylated antibody, increasing the amount of either EndoSd-D232M or G2S2-oxazoline can enhance the transglycosylation efficiency. When the amount of EdoSd-D232M was increased by 5-fold, only 60% Herceptin-2N-G2S2 was produced, which did not achieve our expected efficiency (>90%). We then increased the G2S2-oxazoline/antibody ratio to 80:1; an unstable result of the produced Herceptin-2N-G2S2 in the range of 80−90% was obtained. Finally, the G2S2-oxazoline/antibody ratio of 150:1 was applied, which gave stable and repeatable data. A time-dependent HBGT graph (Figure 3d) showed that the EndoSd-D232M slowly transferred G2S2-oxazoline to N297 (Fc region). In the first 5 min, the amount of Herceptin-1N-G2S2 (∼50%) is still larger than that of Herceptin-2N-G2S2 (∼40%). Subsequently, the amount of Herceptin-2N-G2S2 increased to 80% at 10 min and reached ∼94% at 20 min. The deglycosylation did not occur within the first 60 min. The data demonstrate that EndoSd-D232M possesses lower glycosynthase and deglycosylation activities compared to EndoSz-D234M.

In addition to Herceptin-GlcNAc as an acceptor, we also studied the transglycosylation activity using fucosylated Herceptin-GlcNAc (Herceptin-GlcNAc-F), which can potentially be further applied in antibody-drug conjugation (ADC). Using the best transglycosylation conditions described earlier, 94.29 and 94.75% Herceptin-2N-G2S2F were obtained utilizing EndoSz-D234M and EndoSd-D232M, respectively (Table 1), demonstrating that both enzymes have transglycosylation activities on fucosylated substrates.

In conclusion, we have demonstrated that EndoSz-D234M has a transglycosylation activity better than that of EndoSd-D232M (Figure 3c,d). EndoSz-D234M can produce >90% Herceptin-2N-G2S2 or Herceptin-2N-G2S2F with only a 20:1 molar ratio of G2S2-oxazoline/antibody, whereas EndoSd-D232M needs a ratio of 150:1 to achieve similar production purity. Detailed investigations of time-dependent HBGT profiles of EndoSd-D232M (Figure 3d) demonstrated that the transglycosylation processes of the two *N*-glycans on Asn297 are catalyzed by EndoSd-D232M in a stepwise manner rather than the simultaneous conjugation of two *N*-glycans. As for EndoSz-D234M, only 10% Herceptin-1N-G2S2 and ∼90% Herceptin-2N-G2S2 were also observed at 5 min, suggesting a quicker stepwise transglycosylation mechanism. The time course of the G2S2-oxazoline/Herceptin ratio versus the percentage of Herceptin-2N-G2S2 obtained is summarized in Table S1.

Transglycosylation on Various Antibodies and Improved ADCC Activities

We have experimentally demonstrated that the homogeneous *N*-glycan platform mediated by EndoSz-D234M is a powerful platform for establishing homogeneous mAbs. Several other mAbs were also selected for the conjugation investigation by this EndoSz-D234M-mediated platform, including OBI-888, Perjeta, Erbitux, Rituxan, OBI-898, Vectibix, Humira, Keytruda, and Bavencio. With the condition of the G2S2-oxazoline/antibody molar ratio of 20:1, the homogeneous glycan platform demonstrated the effective homogeneous glycan conjugation for selected antibodies (Figure 4a). The percentages of fully glycosylated mAbs are OBI-888-G2S2: 87.57%, Perjeta-G2S2: 92.49%, Erbitux-G2S2: 87.92%, Rituxan-G2S2: 97.57%, OBI-898-G2S2: 89.73%, Vectibix-G2S2: 86.12%, Humira-G2S2: 93.68%, Keytruda-G2S2: 75.81%, and Bavercio-G2S2: 90.73%.

To evaluate the effect of homogeneous glycans on different mAbs, we selected five homogeneous antibodies generated with our homogeneous *N*-glycan platform for further ADCC bioassay. All of the ADCC activities of the five homogeneous *N*-glycan antibodies were increased by 3- to 26-fold compared to the original heterogeneous antibodies (Figure 4a). Notably, the glycan-homogeneous OBI-888 increased the ADCC activity by ∼26-fold, indicating that the homogeneous *N*-glycan platform with EndoSz-D234M plays a critical role in the future antibody drug development of OBI-888. In addition, the EndoSz-D234M-based homogeneous *N*-glycan platform is also applicable to other therapeutic antibodies to improve their efficiencies to help develop novel or biosimilar therapeutic antibodies.

Overall Structural Architecture of EndoSz-D234M, a High-Efficiency Glycosynthase

EndoS-D233Q has generally been utilized in antibody re-engineering. Based on our test, the activity of EndoS-D233M is a little better than that of EndoS-D233Q. Therefore, we compare the transglycosylation efficiencies of EndoSz-D234M and EndoSd-D232M with EndoS-D233M, a major ENGase-based glycosynthase. As shown in Table S2, EndoS-D233M needs 50 min to reach maximum conjugation, whereas EndoSz-D234M takes only 20 min to reach maximum conjugation. In addition, EndoSz-D234M needs only 20eq of G2S2 (biantennary glycan type), but EndoS-D233M needs 40eq of G2S2 and EndoSd-D232M needs 150eq of G2S2. Our new enzyme, EndoSz-D234M, exhibits an indeed better transglycosylation efficiency compared to the major ENGase-based glycosynthases, EndoS-D233M and EndoS-D233Q.

Our study has identified EndoSz-D234M to possess an effective transglycosylation activity on therapeutic antibodies

https://doi.org/10.1021/jacsau.4c00004
JACS Au 2024, 4, 2130−2150

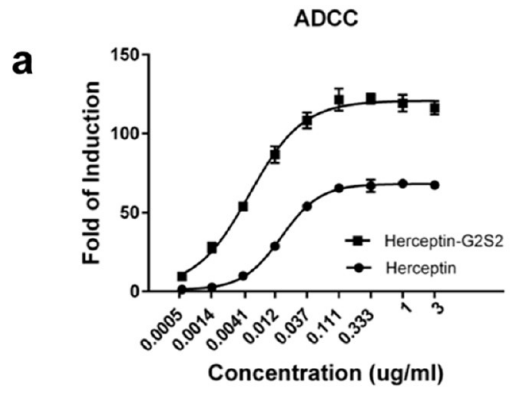

Antibody	GlcNAc	1N-G2S2	2N-G2S2	ADCC Original (EC 50)	ADCC homogeneous (EC 50)
OBI-888	6.33%	6.10%	87.57%	11.92 (μg/ml)	0.45 (μg/ml)
Herceptin	0.44%	8.45%	91.11%	15.29 (μg/ml)	5.10(μg/ml)
Perjeta	0.00%	7.51%	92.49%	23.19 (μg/ml)	3.75 (μg/ml)
Erbitux	2.71%	9.38%	87.92%	8.84 (ng/ml)	0.86 (ng/ml)
Rituxan	0.00%	2.43%	97.57%	42.4 (ng/ml)	3.6 (ng/ml)
OBI-898	0.87%	9.40%	89.73%	-	-
Vectibix	1.56%	13.21%	86.12%	-	-
Humira	0.92%	5.40%	93.68%	-	-
Keytruda	7.65%	16.54%	75.81%	-	-
Bavencio	2.35%	6.95%	90.73%	-	-

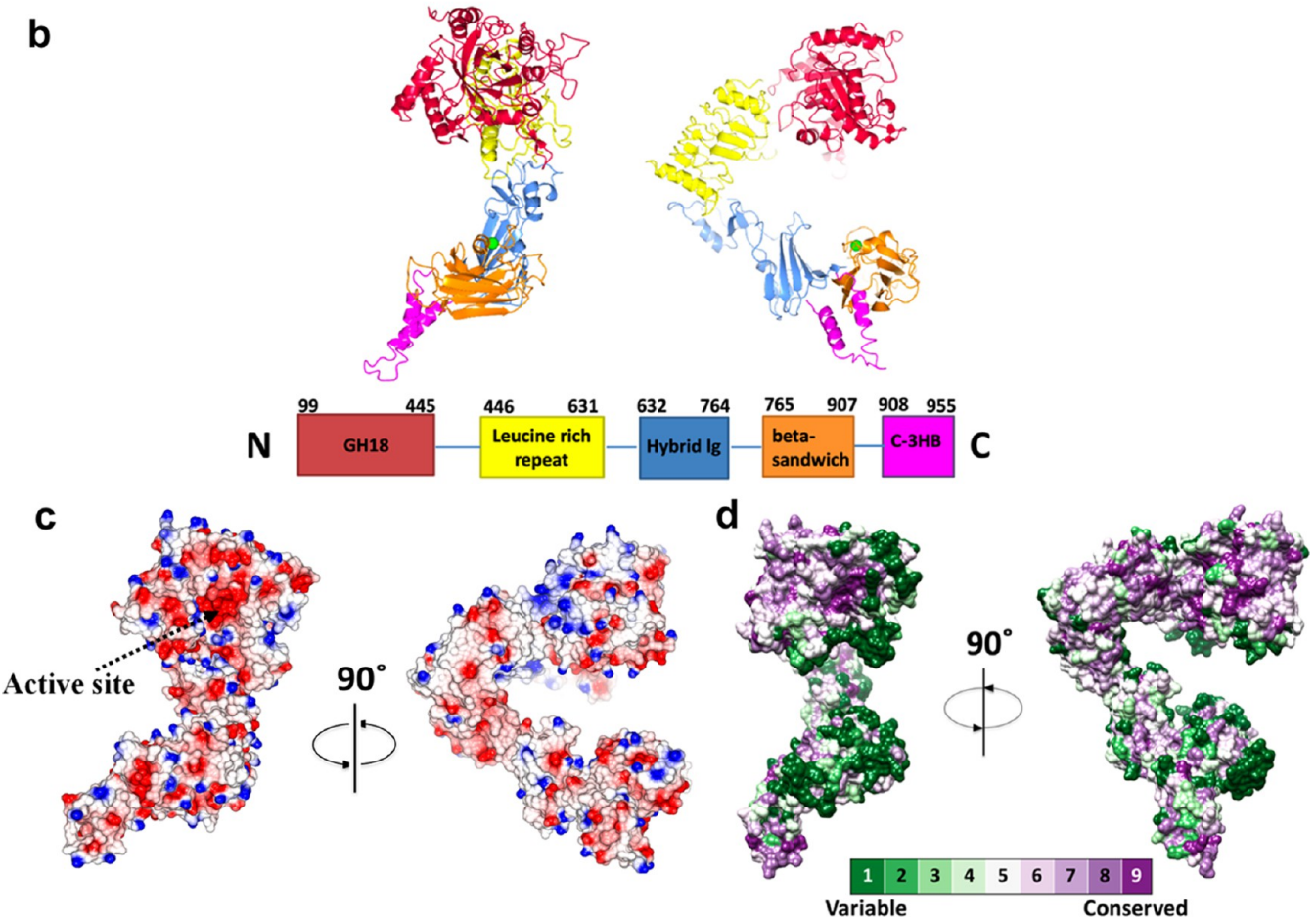

Figure 4. ADCC assay results for original and homogeneous mAbs and overall architecture of apo-EndoSz. (a) The ADCC result of Herceptin and Herceptin-G2S2 is shown in the left panel. The data clearly show that Herceptin-G2S2 exhibits a higher ADCC activity. The EC_{50} values of Herceptin and Herceptin-G2S2 were 15.29 (μg/mL) and 5.10 (μg/mL), respectively. The summary of the transglycosylation efficiency and ADCC in various mAbs is shown in the right panel. (b) Glycosidase (red), leucine-rich repeat (yellow), hybrid Ig (light blue), β-sandwich domain (orange), and C-3HB (purple) domains are shown as a cartoon. The calcium ion is shown as a green sphere. (c) Top and side views of the electrostatic surfaces are shown. (d) Views of the conservation surface of EndoSz.

IgGs and to play a vital role in our homogeneous mAbs platform. To further understand the transglycosylation mechanism, we analyzed the crystal structures of the mutant EndoSz-D234M and the complex with G2S2-oxazoline. Initially, the crystallization of the full-length EndoSz-D234M (a.a. 20−1011) was attempted but failed. Considering that the N-terminal three-helix bundle (N-3HB) caused protein oligomerization, as previously suggested in the case of EndoS,[41] and the C-terminal region might exhibit a flexible character, we designed the truncated EndoSz-D234M with amino acids 99−974 (ΔEndoSz-D234M) for crystallization and X-ray structure determination. As a result, the truncation of EndoSz-D234M successfully led to the acquisition of diffraction-quality crystals with two space groups $P2_12_12_1$ and $P2_1$. Crystals of $P2_12_12_1$ diffracted to a higher resolution of 2.2 Å, compared to $P2_1$ crystals at 3.1 Å. The determined

https://doi.org/10.1021/jacsau.4c00004
JACS Au 2024, 4, 2130−2150

structures of the two crystal forms show similar structural architectures with root-mean-square deviation (RMSD) of 0.75 Å for the Cα atoms without significant conformational variations. Therefore, the structure of ΔEndoSz-D234M with the space group $P2_12_12_1$ at a higher resolution is referred to throughout the manuscript. In both crystal forms, the asymmetric unit contains only one ΔEndoSz-D234M molecule without strong interactions with nearby symmetric molecules (complex significance scores (CSSs) calculated by the PISA server are all 0), corresponding to a monomeric form in the solution state validated by size-exclusion chromatography (Figure S4).

The crystal structure of ΔEndoSz-D234M reveals a monomeric V-shaped architecture, comprising five major domains: a glycoside hydrolase (GH) domain (a.a. 99−445), a leucine-rich repeat domain (446−631), a hybrid Ig domain (632−764), a β-sandwich domain (765−907), and a C-terminal 3-helix bundle domain (908−955) (Figure 4b). One calcium ion (Ca^{2+}) is coordinated in the β-sandwich domain, whose function is discussed in the next section. The active site of the GH domain shows a highly negatively charged surface area with conserved residues (Figure 4c), resulting in possessing highly conserved catalytic residues and the environment for the specific endo-β-*N*-acetylglucosaminidase activity (Figure 4d). However, some loops surrounding the active site of the GH domain and the β-sandwich domain show more variable residues on the surface (Figure 4c). Together with that, the GH and β-sandwich domains, located at the opposite terminus of the V-shaped architecture, face the same plane (Figure 4b). The β-sandwich domain might facilitate or orientate EndoSz to target *N*-glycans of IgG via binding to the given location on the IgG protein for further *N*-glycan cleavage or conjugation.

As shown in Figure S5a,b, the β-sandwich domain of EndoSz-D234M starts from a β-strand (a.a. 769−772) and a helix-turn motif (a.a. 777−791), followed by a typical β-sandwich structure that comprises two antiparallel β-sheets. The six coordinated ligands of the bound Ca^{2+} are side chains of Asp785, Asn790, and Glu901 and main-chain carboxyl groups of Lys782, Leu787, and Pro900 (Figure S6b). We surmise that Ca^{2+} might serve a role as that in the repeat-in-toxin (RTX) motif to induce a disorder-to-order transition, promoting secondary-structure formation in the extracellular space with a high concentration of Ca^{2+}.[48] Compared to other domains, the β-sandwich domain of EndoSz is a highly variable region based on sequence alignment and conservation analyses (Figures 2, S5a, and 4d). The β-sandwich domains of ENGases are suggested to adjust the structural orientation of ENGases to bind the specific carbohydrates or proteins to perform the *N*-glycan cleavage. The sequence variations of β-sandwich domains might be related to the selectivity of the recognized substrates. A structural comparison of the β-sandwich domain of EndoSz-D234M with those of EndoS and EndoS2, however, shows that all β-sandwich domains exhibit a similar structural motif and topology (Figure S5c) despite the significant sequence variations (Figure S5a), suggesting that EndoSz-D234M might target proteins through the β-sandwich domain with the binding approach similar to EndoS and EndoS2 in terms of structural fit but not sequence identity.

Structural Analysis of EndoSz-D234M in Complex with the G2S2-Oxazoline Intermediate

We crystallized *apo*-ΔEndoSz-D234M in two crystal forms of $P2_12_12_1$ and $P2_1$ with resolutions 2.2 and 3.1 Å, respectively (Figure S6a). Initially, we tried to soak G2S2-oxazoline into the $P2_12_12_1$ crystals of higher resolution with a combination of various soaking periods and the soaking concentrations of G2S2-oxazoline but in vain. Therefore, we turned to soak G2S2-oxazoline in the lower-resolution $P2_1$ crystals. Interestingly, we could observe the extra election density of the *N*-glycan in the GH domain at 3.1 Å, a similar resolution to *apo* $P2_1$ crystals. However, the resolution could not be further improved after several optimization trials. Finally, we utilized a novel pH-jump method to obtain the endoSz/G2S2-oxazoline complex structure with high resolution ∼2.3 Å from the crystals of $P2_12_12_1$ (Figure S6b).

With the high-resolution data, the extra density at the GH domain is identified with sufficient quality to allow us to build all 10 moieties of the G2S2-oxazoline (Figure S7a). As mentioned previously, the structure of the GH domain of EndoSz reveals a typical $(\alpha/\beta)_8$-TIM-barrel fold, a cyclic 8-fold repeat of the β-strand/loop/α-helix composition. The bound G2S2-oxazoline consists of Manβ1−4GlcNAc-oxazoline and two glycan antennas α (1−3) and α (1−6) in the $(\alpha/\beta)_8$-barrel and is surrounded by loops on the top of the barrel (Figure S7b). The nomenclature of CT *N*-glycan utilized in the soaking experiment is shown in Figure S7c. The two sugar moieties, Manβ1−4GlcNAc-oxazoline, of the G2S2-oxazoline are located in the cavity formed by the flanked loops and the β-barrel core (Figure S7b). As shown in Figure S7b, the loops connecting α-helices and β-strands can be annotated as loop1 (β1-β2; a.a. 121−146), loop2 (β2-α1; 152−159), loop3 (β3-α2; 186−207), loop4 (β4-α3; 236−248), loop5 (β5-α4; 282−291), loop6 (β6-α5; 305−326), loop7 (β9-α8; 348−380), and loop8 (β10-α9; 402−429).

In addition to Manβ1−4GlcNAc-oxazoline, two glycan antennas α (1−3) and α (1−6) interact with the flanked loops, respectively. Compared to antenna α (1−3), antenna α (1−6) sits more closely near the cavity edge formed by the GH domain and possesses more interactions with the GH domain (Figure S7b). Loops 3 and 4 of the GH domain interact with antenna α (1−6), whereas loops 1, 2, and 7 interact with antenna α (1−3). Moreover, the conservation analysis of the flanked loops shows that loop4, loop6, loop7, and loop8 are the more variable regions (Figure S7d).

Structural Insights into Substrate Specificity of EndoSz-D234M

The complex structure shows that G2S2-oxazoline utilizes its NAG-oxazoline and the trimmanose core to mainly interact with EndoSz-D234M. These interaction regions are conserved in the CT and high-mannose *N*-glycan, suggesting the substrate specificity of EndoSz is not dominated by the protein−carbohydrate interactions. Instead, it could be dominated by the steric accommodation of the substrate to select bi- or triantennary oligosaccharides. As shown in Figure S8a,b, the superimposed complex structures of EndoSz/G2S2-oxazoline and EndoS2/HM-N-glycan show that loop4 (β4-α3; a.a. 236−248) of EndoSz exhibits steric hindrance for the third branch, α (1−3)-linked Man on the α (1−6) antenna, of the HM-N-glycan. Compared to EndoS2, helix α3 (a.a. 248−265) is tilted about 9° and loop4 is four residues longer in EndoSz-D234M, resulting in the structural hindrance of loop4 for

https://doi.org/10.1021/jacsau.4c00004
JACS Au 2024, 4, 2130−2150

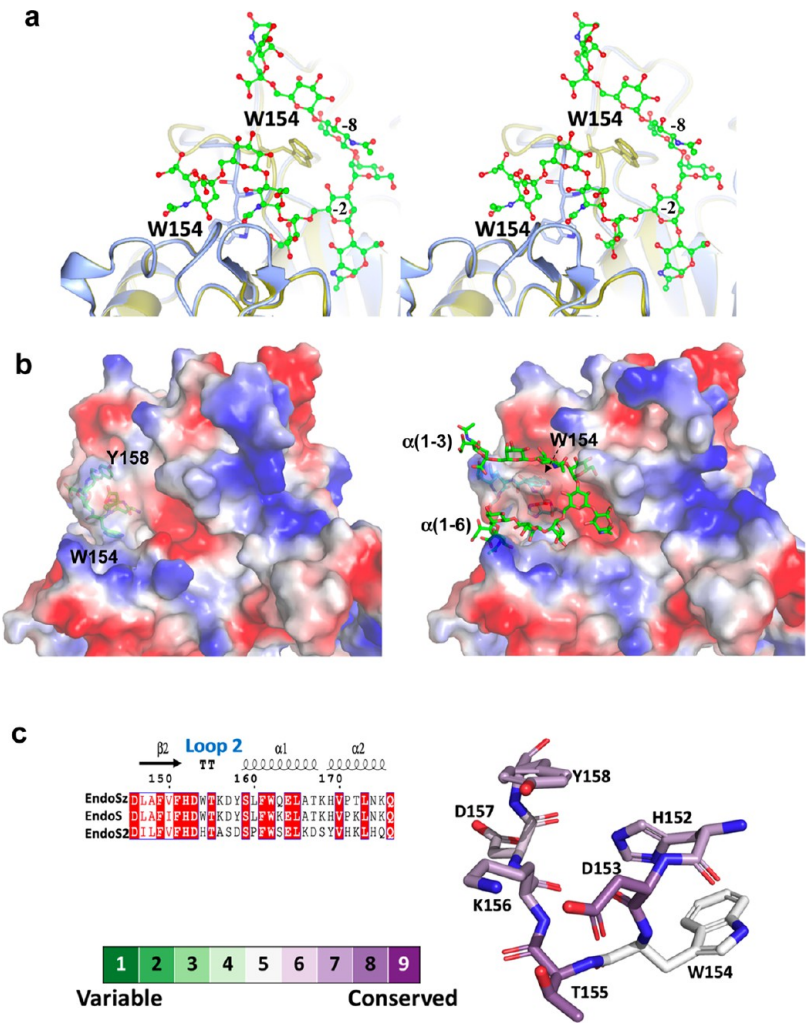

Figure 5. Movement of loop2 reshapes the two binding grooves after *N*-glycan binding. (a) Stereo view of the superimposed structures of *apo*- and *holo*-EndoSz-D234M. The *apo*-EndoSz-D234M (blue) and *holo*-EndoSz-D234M (gold) are shown as a cartoon. The bound G2S2-oxazoline in the *holo*-EndoSz-D234M is shown as balls and sticks. The key residues W154 (sticks) and interacted Man (−2) and NAG (−8) are labeled. (b) Electrostatic surfaces of the unbound (left) and the G2S2-oxazoline bound (right) EndoSz-D234M structures. Loop2 (H152−Y158) and G2S2-oxazoline (right, green) are shown as sticks. W154 and Y158 are labeled. (c) Sequence alignment and the conservation plot of loop2 of EndoSz-D234M.

accommodating HM-N-glycan. The conformations of loop4 of EndoS2/HM-*N*-glycan and unbound EndoS2 are the same, indicating that the structural variations of loop4 between EndoS2 and EndoSz-D234M are inherent and specific for HM-*N*-glycan and G2S2-oxazoline, respectively. The structural variations of helix3 and loop4 between EndoSz-D234M and EndoS2 could dominate the substrate-sugar selectivity.

Mobile Loop2 Forms Two Accommodated Grooves for Each Antenna

A structural comparison of *apo* and *holo* ΔEndoSz-D234M shows that loop2 (a.a. 152−159) exhibits conformational variations (Figure 5a,b). In the apo-EndoSz-D234M structure, Trp154 and Arg182 form a typical cation−pi interaction (Figure S9).[49] However, upon the structural alteration of loop2, Trp154 flips its side chain to interact with the Man (−2) of the core disaccharides and NAG (−8) with a hydrogen bond and the weak carbohydrate−aromatic interaction, respectively, in the *holo* ΔEndoSz-D234M structure. This movement of loop2 reshapes the asymmetric grooves in the GH domain to accommodate two antennas of G2S2-oxazoline (Figure 5b). Moreover, the crystal structure of *apo*-ΔEndoSz-D234M of $P2_1$ (PDB entry 8W4I) at the acid condition shows that Trp154 still interacts with Arg182 via a cation−pi interaction, indicating that the movement of loop2 results from the binding of G2S2-oxazoline rather than an effect of the pH environment. The phenomena of the mobile loop2 are also observed in structures of EndoS and EndoS-CT-*N*-glycan (PDB entries 4NUY and 6EN3) but not in structures of EndoS2 and EndoS2-CT-*N*-glycan (PDB entries 6E58 and 6MDS) (Figure S10). EndoSz-D234M and EndoS both possess the same tryptophan residue (Trp154 of EndoSz) in loop2, whereas the analogue residue of EndoS2 is the histidine residue (Figure 5c), which could result in different substrate-binding mechanisms. Notably, the groove of EndoSz is narrower than that of EndoS2, leading to broad-spectrum substrates for EndoS2. In addition, the flanked residues of Trp154, i.e., His152, Asp153, and Thr155, are highly conserved (Figure 5c), highlighting the importance of Trp154 of EndoSz-D234M.

https://doi.org/10.1021/jacsau.4c00004
JACS Au 2024, 4, 2130−2150

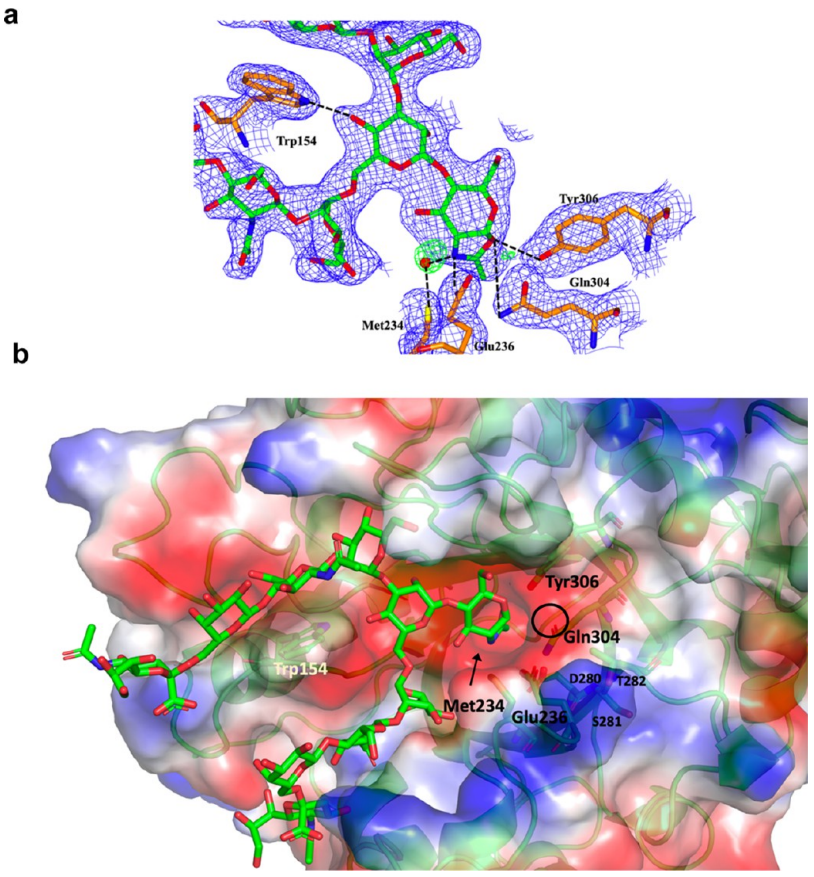

Figure 6. Important H-bonding network around the core of the bound G2S2-oxazoline. (a) The $2F_o - F_c$ electron density map (blue meshes, contoured at 1.0 σ) and the $F_o - F_c$ omit map (green meshes, contoured at 3.0 σ) are shown. The interaction residues with G2S2-oxazoline of EndoSz are labeled and shown as orange sticks. The bound water mediating oxazoline nitrogen and Met234 of EndoSz is shown as the red sphere. (b) Electrostatic surface of the EndoSz-D234M/G2S2-oxazoline structure. The extra space in the groove (black arrow) and the space (black circle) are expected to accommodate the acetamido group of NAG (−1) and NAG (+1), respectively. The residues (sticks) involved in the H-bonding network around NAG-oxazoline are labeled with a larger black font, whereas the residues (sticks) in the presumably Asn-NAG (+1) binding region are labeled with a smaller black font. Trp154 is labeled with a wheatish font.

Detailed Interactions between EndoSz-D234M and G2S2-Oxazoline

The bound G2S2-oxazoline intermediate utilizes the NAG-oxazoline (−1) and the trimanose core (−2, −3, and −7) to make major contacts with EndoSz-D234M. Herein, NAG-oxazoline (−1), with a clear electron density, possesses the H-bonding network with Met234, Glu236, Gln304, Tyr306, and a bound water molecule within the activity site (Figure 6a). A small hole, named an oxa-hole, composed of Met234, Glu236, Gln304, F151, Tyr306, Tyr118, and Tyr401, of which Tyr118 is located at the bottom and others surround the hole, accommodates the terminal C8 atom of oxazoline to stabilize the G2S2-oxazoline intermediate. Structurally, other ENGases, such as EndoS and EndoS2, also possess oxa-holes, suggesting the oxa-holes are important for the accommodation of oxazoline intermediates of ENGses besides EndoSz. The acetamido groups of NAG (−1) of EndoS2/CT-*N*-glycan sit inside the oxa-hole and that of EndoS/CT-*N*-glycan is partially located inside the oxa-hole, suggesting that the oxa-hole is the place for the transition of substrates, intermediates, and products. The pyranose ring of NAG-oxazoline exhibits a $^4C_1$ conformation to sit inside the negatively charged groove (Figure 6b). Notably, the groove provides extra space for the acetamido group of NAG (−1) after transglycosylation is further catalyzed by EndoSz-D234M and the oxazoline ring is open. The extra space and the oxa-hole could provide space flexibility for the transition states between NAG (−1) and NAG-oxazoline (Figure 6b). The oxazoline nitrogen interacts with Met234, Glu236, and a bound water molecule, whereas the oxazoline oxygen interacts with Gln304 and Tyr306. The detailed interactions between EndoSz-D234M and the G2S2-oxazoline intermediate are shown in Figure 7.

The O2 atom of Man (−2) forms a hydrogen bond with Trp154. The O2 and O3 atoms of Man (−3) and the O7 atom of NAG (−4) have hydrogen bonds with the side chain of Arg187. For Man (−7), the hydrogen bonds, Man (−7)-O3/Trp122, Man (−7)-O4/Arg120, and Man (−7)-O6/Asn357, are clearly observed. The major hydrogen-bond interactions between the G2S2-oxazoline and Δ*E*ndoSz-D234M result from the four moieties:—NAG-oxazoline (−1), Man (−2), Man (−3), and Man (−7) of the pentasaccharide core. GlcNAc (+1) is not involved as the substrate G2S2-oxazoline does not contain this moiety. Interestingly, these hydrogen-bonding residues, except for Arg187 and Trp154, are all conserved among EndoSz, EndoSd, EndoS, and EndoS2, highlighting the unique roles of Arg187 and Trp154. In addition, GlcNAc (−8) on antenna α (1−3) possesses a carbohydrate−aromatic interaction with Trp154. However, GlcNAc (−4) on antenna α (1−6) possesses a weak carbohydrate−aromatic interaction with His194 and a hydro-

https://doi.org/10.1021/jacsau.4c00004
JACS Au 2024, 4, 2130−2150

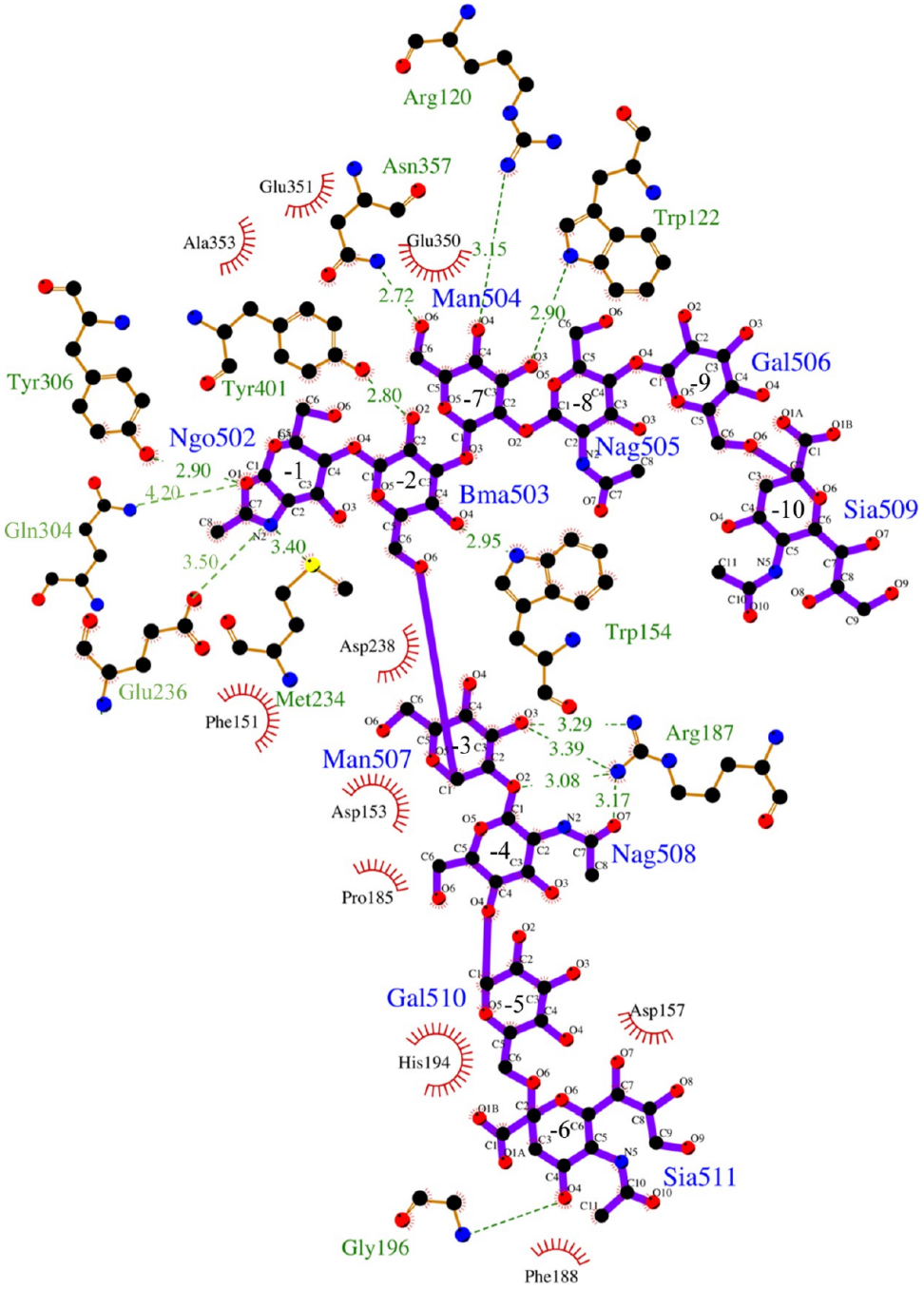

Figure 7. 2D diagram of EndoSz-D234M/G2S2-oxazoline interactions. The bound G2S2-oxazoline is shown as purple sticks. The interacting residues of EndoSz-D234M with hydrogen bonds (green dashed lines) and hydrophobic interactions are shown as orange sticks and red eyes, respectively. Gln304, 4.2 Å distant from the oxazoline oxygen, forms a weak hydrogen bond with the oxazoline oxygen.

gen bond with Arg187. These are the minor contacts between D234M-EndoSz and the bound CT *N*-glycan mediated by GlcNAc (−8) and GlcNAc (−4).

Mutagenesis Studies of Transglycosylation Activities of EndoSz and EndoSd Based on EndoSz/G2S2-Oxazoline Complex Structures

To explore and develop more effective EndoSz with transglycosylation activity, systematic site-directed mutagenesis studies on Asp234 of the conserved catalytic motif, $D^{229}xxD^{232}xD^{234}xE^{236}$, its structurally nearby residues (T183 and D232), and the presumable Asn-GlcNAc (+1)-binding region (D280, S281, and T282) were performed (Figure 8a,c). In addition, previous studies showed that EndoS-D233Q and EndoS2-D184M (analogue residue D234 in EndoSz) could increase the transglycosylation activity for the specific glycan.[27,35] Recently, Shivatare et al. demonstrated that the EndoS2-T138Q (analogue residue T180 in EndoSz) and EndoS2-D226Q (analogue residue D280 in EndoSz) mutants exhibited transglycosylation activities better than EndoS2-D184M.[47] According to a multiple-sequence analysis (Figure 2), the important and nearby residues, i.e., T183, D232, D234, D280, S281, and T282 of EndoSz and T181, D230, D232, D278, S279, and T280 of EndoSd, at equivalent positions of the above-mentioned mutated sites were selected as primary

https://doi.org/10.1021/jacsau.4c00004
JACS Au 2024, 4, 2130−2150

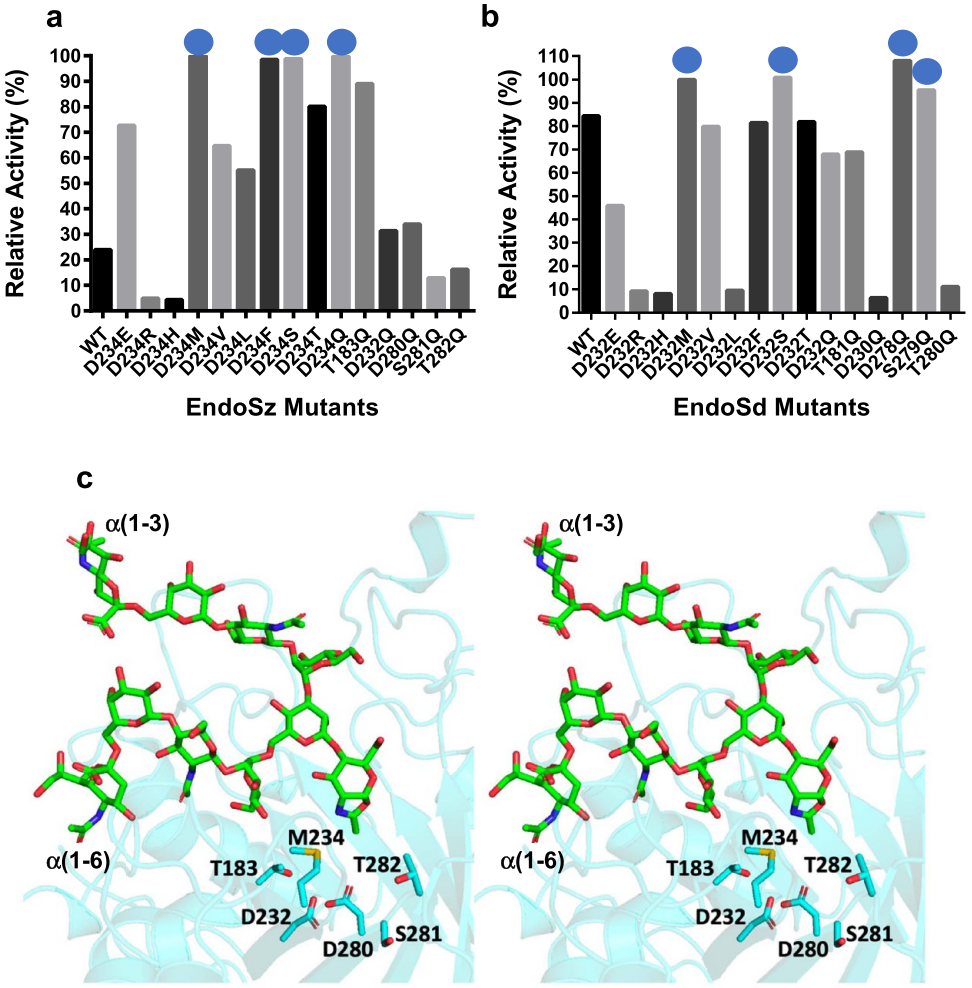

Figure 8. Mutagenesis and structural studies of D234 mutants and nearby selected residues for transglycosylation activities. (a) EndoSz. (b) EndoSd. The activities were calculated by the product percentage of Herceptin-2N-G2S2 plus 1/2 Herceptin-1N-G2S2. (b) Structural presentation of the selected mutants for studies of the transglycosylation activity. Mutants with significantly enhanced transglycosylation activities compared to wild-type EndSz and EndoSd are labeled with blue spheres. (c) Stereo view of the structural presentation of the selected mutants for studies of transglycosylation activity.

targets for the site-directed mutagenesis investigation, among which D234 of EndoSz and D232 of EndoSd at the catalytic sites exhibit key roles in activities. Since D234 of EndoSz is structurally involved with the hydrogen network with the oxazoline nitrogen in our complex structure, D234 of EndoSz and D232 of EndoSd were hence further substituted with several different mutant types, including positively/negatively charged and polar/nonpolar residues. The transglycosylation activities of the mutant enzymes were assessed using the best conditions described earlier.

As shown in Figure 8a, assays of the transglycosylation activities of EndoSz mutants show that EndoSz-D234M exhibits the highest activity (relatively set to 100%), and EndoSz-D234Q (99.9%), EndoSz-D234S (98.8%), and EndoSz-D234F (98.6%) have sequentially high activities. In contrast, EndoSz-D234R (4.9%) and EndoSz-D234H (4.5%) have low activities. The wild-type EndoSz also has a slight transglycosylation activity (24.3%). Besides mutations on the D234 position, EnodSz-D232Q (31.4%), EndoSz-D280Q (34.0%), EndoSz-S281Q (12.9%), and EndoSz-T282Q (16.3%) have no significantly enhanced transglycosylation activity, except for EndoSz-T183Q (89.1%), compared to EndoSz-D234M.

As for EndoSd mutants (Figure 8b), EndoSd-D232M (relatively set to 100%), EndoSd-D232S (100.8%), and EndoSd-D278Q (108.0%) all have high transglycosylation activities, whereas EndoSd-D232R (9.2%) and EndoSd-D232H (8.1%) both have low activities. Comparably, the wild-type EndoSd has a relatively high transglycosylation activity (84%). The profiles of the transglycosylation activity changes of the key residues in the active site for EndoSz-D234 and EndoSd-D232 variants are similar, except for D232V, D232L, D232F, and D232Q in EndoSd.

In conclusion, EndoSz-D234M and EndoSd-D278Q are shown to exhibit the best transglycosylation activities on Herceptin-GlcNAc to produce homogeneous Herceptin bearing the desired *N*-glycans at the Fc region. EndoSz-D234M shows a higher transglycosylation activity from EndoSz-WT in comparison to EndoSd-D232M from EndoSd-WT. In contrast to D234 in EndoSz, the variations of transglycosylation activities show enormously different profiles with mutations at structurally nearby residues (T183 and D232 in EndoSz) and the presumable Asn-GlcNAc (+1)-binding

https://doi.org/10.1021/jacsau.4c00004
JACS Au 2024, 4, 2130−2150

Table 2. Conjugation Investigation of Various Sugars with EndoSz-D234M[a]

acceptor	glycan type	conjugation		
		GlcNAc(F)	1N-glycan	2N-glycan
Herceptin-GlcNAc	M3(40eq)	1.11%	6.51%	92.37%
	G0(20eq)	0.91%	2.58%	96.50%
	G2(20eq)	0.61%	4.52%	94.87%
Herceptin-GlcNAc-F	M3F(20eq)	0.62%	4.95%	94.44%
	G0F(20eq)	0.00%	2.45%	97.55%
	G2F(20eq)	0.21%	2.64%	97.14%

[a]The portions of products GlcNAc(F), 1N-G2S2, and 2N-G2S2 were recorded when the transglycosylation reactions using various sugar substrates were performed with EndoSz-D234M under the transglycosylation condition (G2S2-oxazoline/antibody ratio of 20:1 (20eq) with 10 min reaction time). However, the transglycosylation reaction conjugating M3 to Heceptin-GlcNAc was performed under the transglycosylation condition (G2S2-oxazoline/antibody ratio of 40:1 (40eq) with a 10 min reaction time).

region (D280, S281, and T282 in EnodSz). For example, D232Q and D280Q in EndoSz exhibit similar transglycosylation activities (~30%), whereas D230Q and D278Q at the equivalent positions in EndoSd show very low (~5%) and high activities (108.0%), respectively.

All mutants with the replacement of Asp234, except for D234R and D234H, exhibit enhanced transglycosylation activities. Among these mutants, four mutants D234M, D234F, D234S, and D234Q possess the best relative transglycosylation activity (~100%). A detailed investigation of the structural roles of these mutated residues shows that Met234 shares a hydrogen bond mediated by a bound water molecule with the oxazoline nitrogen (Figure 6a). D234S and D234Q mutants could exhibit excellent transglycosylation activities in a similar manner. Interestingly, D234F also exhibits a great transglycosylation activity, suggesting that a weak water-mediated hydrogen bond (OH···π) is sufficient for good transglycosylation at this position. However, D234R and D234H, with positively charged side chains, could hinder the water-mediated hydrogen bond with the oxazoline nitrogen. Moreover, the residues at positions 280 and 281 of EndoS (analogue residues 281 and 282 of EndoSz) were previously proposed to have interactions with GlcNAc (+1).[42] Herein, D280Q (34%), S281Q (12.9%), and T282Q (16.3%) do not possess significantly different transglycosylation activities, compared to the wild-type EndoSz (24.3%), suggesting that the hydrogen-bond pattern between EndoSz and the bound G2S2-oxazoline is more important for the transglycosylation activity than that between EndoSz and the target Asn-GlcNAc (+1). In contrast, D278Q (108.0%), S279Q (~92%), and T280Q (~10%) of EndoSd show different profiles of transglycosylation activities in the presumable Asn-GlcNAc (+1)-binding region, suggesting EndoSz and EndoSd could possess different transglycosylation mechanisms for the recognition of Asn-GlcNAc (+1) of IgG-Fc.

Structural Insights into Conjugation of EndoSz-D234M on Various Sugars

Our data indicate that the EndoSz- and EndoSd-based homogeneous *N*-glycan platforms can well process all different types of *N*-glycans, including G2S2, G2, G0, M3, G2S2F, G2F, G0F, and M3F, to produce homogeneous therapeutic antibodies (Tables 1 and 2). G0 and G2 could reach >90% fully glycosylated Herceptin before deglycosylation with a molar ratio of 20:1 (G2S2-oxazoline/antibody), whereas M3 reached 92.3% fully glycosylated Herceptin with the conjugation parameters of 40:1 molar ratio (G2S2-oxazoline/antibody) and 10 min reaction time. Similar experiments were applied to fucosylated Herceptin-GlcNAc (Herceptin-GlcNAc-F). The results showed that all glycans, including M3, were able to be conjugated with high efficiency (>90%) in a 20:1 molar ratio (G2S2-oxazoline/antibody).

Among these *N*-glycans, the transglycosylation activity with M3 is the lowest, indicating the importance of three terminal glycans, which are lacking in M3. We believe that the terminal three glycans, *N*-acetylglucosamine, galactose, and sialic acid, increase the transglycosylation activity through an enhancement of the binding ability of *N*-glycans to EndoSz-D234M (Figure 1). Compared to G0, the additional galactose (G2) and sialic acid (G2S2) did not improve the transglycosylation activity, agreeing with the fact that the terminal galactose (−5 and −9) and sialic acid (−6 and −10) did not contribute to the binding in our complex structure. Interestingly, in the absence of minor interactions between GlcNAc (−8) and Trp154, GlcNAc (−4) and His194, and GlcNAc (−4) and Arg187, the transglycosylation activity with M3 is lower than that with G0, highlighting the importance of GlcNAc (−8) and GlcNAc (−4) for binding on EndoSz-D234M, compared to G0. Moreover, it is interesting to note that EndoSz-D234M has a higher conjugation activity on Herceptin-GlcNAc-F than Herceptin-GlucNAc for all glycans, M3, G0, G2, and G2S2, suggesting that the fucose group contributes to the stabilization of the EndoSz-D234M/glycan complex binding enhancement for further transglycosylation reaction.

Closed- and Open-Form IgG-Fc in the Presence of EndoSz-D234M

IgG-Fc serves as a critical receptor for activating immune effector functions, such as ADCC and CDC. The glycoforms on the IgG-Fc affect the structural integrity of IgG-Fc to dominate the binding of the effector ligands, such as Fc γ receptors (FcγRs)[11,50−53] or the complement factor (C1q).[54] EndoSz-D234M plays an important role in glycosylation engineering to manipulate the glycoforms on IgG-Fc. To understand how EndoSz-D234M interacts on IgG-Fc, the cocrystallization experiment of EndoSz-D234M with human IgG-Fc in various ratios was performed as EndoSz-D234M possesses a low hydrolysis activity on the *N*-glycans of IgG-Fc. However, all of the determined structures from rice-shaped crystals showed only the dimeric IgG-Fc (Table S3 and Figure S11a). The determined IgG-Fc structure exhibits a typical horseshoe-like structure, of which the CH2 domain exhibits the conformation in a closed form. Interestingly, the electron densities of two *N*-glycans on the dimeric IgG-Fc were clearly defined. One of the two *N*-glycans on the IgG-Fc showed a weaker electron density (Figure S11b,c). Molecular docking of

https://doi.org/10.1021/jacsau.4c00004
JACS Au 2024, 4, 2130−2150

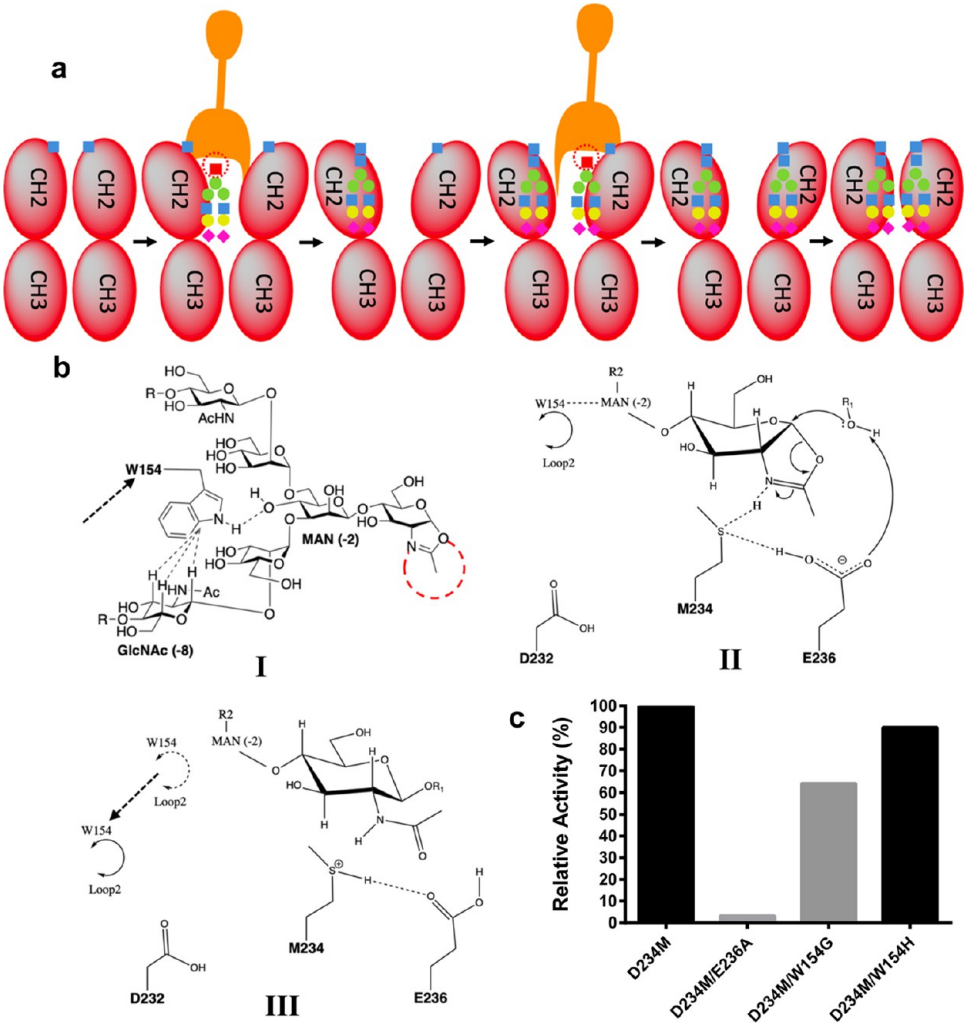

Figure 9. Proposed mechanism of D234M EndoSz-catalyzed transglycosylation. (a) Cartoon diagram describing the stepwise transglycosylation process of EndoSz-D234M. The cartoon representations of EndoSz-D234M (orange) and IgG-Fc (red) are shown. *N*-acetylglucosamine-oxazoline (small red rectangles), *N*-acetylglucosamine (small light-blue rectangles), mannose (small green circles), galactose (small yellow circles), and sialic acid (small pink diamonds) are shown. (b) Transglycosylation catalyzed by EndoSz-D234M. The critical catalytic residues in the active site are numbered. The hydrogen bonds are presented as straight dashed lines. The dashed lines between Trp154 and GlcNAc (−8) represent CH−π interactions. R represents the sugar moieties (−5, −6, −9, and −10). R2 and R1 represent the sugar moieties (−3 to −10) and the target protein with the sugar moiety GlcNAc (+1) on the Asn residue, respectively. The mobile loop2 is labeled. (c) Mutagenesis study of the two key residues, Glu236 and Trp154, in relative transglycosylation activities. D232 is an important residue in deglycosylation but not in the transglycosylation mechanism. The red dashed circles represent structural oxa-holes.

EndoSz-D234M in complex with IgG-Fc, based on the determined locations of *N*-glycans in Δ*E*ndoSz-D234M and IgG-Fc in our structures, shows that the two *N*-glycans are spatially inaccessible for EndoSz-D234M (Figure S12). A large conformational alteration of Fc is thus needed to expose the *N*-glycans for hydrolysis by EndoSz or transglycosylation by EndoSz-D234M as IgG-Fc was suggested to possess considerable motion.[55]

Moreover, after a long period of crystallization incubation (18 months) at 18 °C, the cuboid crystals, rather than rice-shaped crystals, were grown. The determined structure from the cuboid crystal also showed only IgG-Fc. However, surprisingly, the IgG-Fc structure exhibits an open form (Figure S13a), rather than a closed form, in the CH2 domain, which allows accommodating EndoSz-D234M for the *N*-glycan transglycosylation or cleavage. The closed and open conformations of IgG-Fc in the presence of EndoSz-D234M were grown in similar crystallization conditions (100 mM MES, pH 6, 200 mM zinc acetate, and 10% PEG8000; 100 mM MES, pH 6.5, 200 mM zinc acetate, and 10% PEG8000, respectively). What triggers a large conformational change of the CH2 domain of IgG-Fc is not clear. However, such a structural alteration is necessary for EndoSz-D234M to access *N*-glycans on the CH2 domain of IgG-Fc. The temperature *B*-factor distribution of the closed-form IgG-Fc structure exhibits an asymmetric dynamic property in the CH2 domain (Figure S13b); together with a larger movement in only one of the two CH2 domains (∼11 Å) (Figure S13c), the transition from the closed to the open form of the IgG could behave in an asymmetric manner.

Proposed Stepwise Transglycosylation Mechanism

Based on the CryoEM structure of EndoS with the open-form IgG-Fc (PDB entry 8A64), reasonable docking for the complex structure of EndoSz-D234M with the open-form IgG-Fc is performed. The β-sandwich domain of EndoSz-D234M

https://doi.org/10.1021/jacsau.4c00004
JACS Au 2024, 4, 2130−2150

interacts with IgG-Fc. With the model, NAG (+1) of Fc must flip out to perform the transglycosylation reaction (Figure S14);[56] otherwise, the distance between NAG (+1) of IgG-Fc and the carried NAG-oxazoline is too far to perform the transglycosylation reaction. The conformation alternation of the open-form IgG-Fc is also needed to expose the NAG (+1). The open-form IgG-Fc cannot accommodate two EndoSz-D234M simultaneously, confirming the stepwise behavior observed in the study of transglycosylation activities of EndoSz-D234M and EndoSd-D232M (Figure 3c,d). As shown in Figure 9a, the stepwise transglycosylation mechanism of EndoSz-D234M is proposed. For the occurrence of transglycosylation behavior with EndoSz-D234M, a large conformational alternation is necessary for the closed-form IgG-Fc. To conquer the steric hindrance, some unknown factors might trigger a conformational change of the closed-form IgG-Fc, which needs further investigation. The transition from a closed to an open form of IgG-Fc is mediated by the CH2 domain in an asymmetric manner. The asymmetric movement might provide more accessibility to the first Asn297 to facilitate the first-*N*-glycan transglycosylation. Subsequently, the first EndoSz-D234M leaves and the second EndoSz-D234M carries the secondary *N*-glycan to perform the secondary transglycosylation. After the establishment of the two *N*-glycans on IgG-Fc, EndoSz-D234M leaves. The fully glycosylated IgG-Fc returns to the closed form, which could avoid the hydrolysis of *N*-glycan, whereas EndoSz-D234M still possesses a low ability to perform *N*-glycan hydrolysis. In contrast, EndoSz could also follow the stepwise mechanism to perform the hydrolysis of *N*-glycans on IgG-Fc.

To understand the transglycosylation mechanism of EndoSz, we mutated the catalytic motif $D^{229}xxD^{232}xD^{234}xE^{236}$ to $D^{229}xxD^{232}xM^{234}xE^{236}$ and determined the structures of apo-EndoSz-D234M and its complex form with G2S2-oxazoline (EndoSz/G2S2-oxazoline). Our study has demonstrated that EndoSz-D234M exhibits an excellent transglycosylation activity. A detailed structural investigation of the EndoSz/G2S2-oxazoline complex shows a clear electron density of NAG-oxazoline (−1), indicating that the G2S2-oxazoline, the enzymatic reaction intermediate, is not hydrolyzed, while the intact oligosaccharide is carried by EndoSz-D234M.

Based on the structures of apo-EndoSz-D234M and its complex with G2S2-oxazoline, we propose a transglycosylation mechanism catalyzed by EndoSz-D234M (Figure 9b). First, especially in the acid condition, in step I, loop2 of EndoSz-D234M moves close to the branched point of the two antennas of the transferred sugar. Trp154 on loop2 forms a hydrogen bond with O4 of Man (−2) and a carbohydrate−aromatic interaction with GlcNAc (−8). Together with the stabilization of NAG-oxazoline in the oxa-hole at one end of G2S2-oxazoline, the large movement of loop2 could further stabilize the transferred sugar (G2S2-oxazoline) at the other end for transport to the target Asn297 of the acceptor protein and for further glycosidic-bond formation. From a previous structural report on endoglycosidases,[42] Asp233 in EndoS, the analogous residue of Asp234 of EndoSz, formed a hydrogen bonding with Asp231 in EndoS, the analogous residue of Asp232 of EndoSz, in the resting state, and Asp233 in EndoS exhibited a large side-chain conformational change upon binding of the substrate sugar for substrate-assisted hydrolysis. Interestingly, the mutated residue Met234 of EndoSz-D234M, without the hydrogen bond with Asp232 in the resting state, does not exhibit a significant conformational change upon G2S2-oxazoline binding, which is concluded by our *apo* and *holo* ΔEndoSz-D234M structures. The structural characteristics of D234M might facilitate eliminating the hydrolytic activity and enhancing the transglycosylation activity of EndoSz enormously via the spatial accommodation of free *N*-glycans rather than Asn-linked sugar. The mutated residue Met234 forms a water-mediated hydrogen bond with oxazoline nitrogen. In addition, residues Glu304 and Tyr306 form hydrogen bonds, respectively, with oxazoline oxygen to stabilize the end of NAG-oxazoline in the intermediate state.

The bound G2S2-oxazoline is carried by EndoSz-D234M to the target, Asn-GlcNAc (+1). How EndoSz-D234M targets Asn-GlcNAc (+1) remains unknown, which is presumably mediated by the β-sandwich domain as which EndoS had identified interactions with the CH2-CH3 joint of Fc.[56] According to the structural analysis of the EndoSz-D234M/G2S2-oxazoline complex (Figure 6b), Gln304 and Asp280 might play important roles in accommodating NAG (+1), especially for the acetamido group. T282 might accommodate the Asn residue of Asn-GlcNAc (+1). Subsequently, during step II, the twist-boat NAG-oxazoline with a $^4C_1$ conformation was confirmed in our EndoSz-D234M/G2S2-oxazoline complex structure. The proton is transferred from the Asn residue on the target protein (most likely Asn297 on Fc) to the carboxylic acid residue Glu236 of EndoSz-D234M, activating the acceptor protein to process the transglycosylation. Steps II and III of the proposed transglycosylation mechanism are supported by the works of Withers.[57] In the third step, the carried *N*-glycan of EndoSz-D234M is transferred to the Asn residue of the acceptor protein (Asn297 of Fc). The NAG-oxazoline is subsequently catalyzed into the chair-form NAG (−1) at the location of the oxa-hole. The acetamido group of NAG (−1) is expected to be fully or partially located in the oxa-hole. Finally, loop2 of EndoSz-D234M switches its conformation back to interact with Arg182 of EndoSz-D234M via a cation−pi interaction. The hemi- or fully glycosylated IgG then leaves the active site of EndoSz-D234M.

Interestingly, Asp232 does not play a critical role in the proposed transglycosylation mechanism of EndoSz-D234M from a structural viewpoint (in steps I−III) (Figure 9b), which agrees with our finding of the relative transglycosylation activity of D232Q (31.4%) being similar to that of WT-EndoSz (24.3%) (Figure 8a). In contrast, the analogous variant, D230Q, of EnodoSd shows a very low transglycosylation activity (∼5%), suggesting that EndoSz and EndoSd could have different transglycosylation mechanisms.

D234S (98.8%) and D234Q (99.9%) could exhibit high transglycosylation activities as the mutated Ser234 and Gln234 residues possess similar hydrogen-bond networks with oxazoline nitrogen and Glu236 as observed in D234M (Figure S15). D234S is supposed to share a weaker water-mediated hydrogen bond with the oxazoline nitrogen as a result of the shorter side chain compared to D234M. Interestingly, D234F also exhibits a great transglycosylation activity (98.6%), suggesting that the weak hydrogen bonds between π···H···N (Phe234, water, and oxazoline nitrogen) and C···H···O (Phe234, water, and Glu236) are enough to possess a great transglycosylation activity for EndoSz. As for D234R and D234H, the positively charged side chains of Arg and His residues could hinder the hydrogen-bond networks among Met234, water, and oxazoline nitrogen, resulting in a low transglycosylation activity. Conclusively, the hydrogen-bond networks among the mutated

https://doi.org/10.1021/jacsau.4c00004
JACS Au 2024, 4, 2130−2150

residue Met234, water, oxazoline nitrogen, and Glu236 are critical for the transglycosylation activity of EndoSz-D234M.

However, the strengths of these hydrogen-bond networks cannot be strong. The mutated Val234 (∼65%) and Leu234 (∼55%) could not form hydrogen bonds with oxazoline nitrogen and Glu236, whereas the mutated Asp234 (∼24%) and Glu234 (∼73%) could form strong hydrogen bonds. Therefore, these four variants are not preferred for transglycosylation. Moreover, Thr234, with a short polar side chain as Ser234, could also partially meet the criteria as the relative transglycosylation activity (∼80%) of Thr234 is also high. In addition, the location of T183 is close to Met234; the mutated Q183 could therefore replace the role of Met234 in the hydrogen-bond network via its longer side chain, resulting in a high transglycosylation activity of T181Q (89.1%). These architectures of variants with high transglycosylation activities could accommodate NAG-oxazoline (−1) of G2S2-oxazoline better than NAG (−1) of *N*-glycans on IgG-Fc. As a result, we can only observe the *N*-glycan hydrolysis by EndoSz-D234M at the state of fully glycosylated Herceptin rather than hemiglycosylated Herceptin (Figure 3c,d).

To precisely clarify the proposed transglycosylation mechanism, the double mutations D234M/E236A, D234M/W154G, and D234M/W154H were selected for transglycosylation analyses (Figure 9c). D234M/E236A and D234M/W154G resulted in ∼97 and ∼36% decreased transglycosylation activities compared to EndoSz-D234M, indicating E236 and W154 indeed play vital roles in the transglycosylation activity. E236 is essential for the transglycosylation of EndoSz-D234M, agreeing with the importance of hydrogen-bond networks among M234, water, E236, and oxazoline nitrogen and the role in activating the acceptor IgG-Fc via deprotonation in the proposed transglycosylation mechanism. Without the side chain of W154, the ∼36% decreased transglycosylation activity could result from a reduced accommodation ability or stability of the carried *N*-glycans for further transglycosylation. However, D234M/W154H only resulted in a ∼ 10% decreased transglycosylation activity compared to EndoSz-D234M. We thus surmise that the hydrogen bond between W154 on loop2 and O4 of Man (−2) influences the transglycosylation activity. In the D234M/W154H mutant (∼10% decreased), the imidazole hydrogen of H154 could also form a hydrogen bond with O4 of Man (−2) as in EndoS2 (Figure S10c). The hydrogen bond could stabilize the binding of the carried G2S2-oxazoline to facilitate further the transglycosylation process.

CONCLUSIONS

Our EndoSz-D234M-based homogeneous *N*-glycan platform can effectively process G2S2, G2, G0, M3, G2S2F, G2F, G0F, and M3F glycans. With that, several marketed therapeutic antibodies or those in development, including OBI-888, Herceptin, Perjeta, Erbitus, and Rituxan, are shown to have improved therapeutic efficiencies in terms of ADCC. To further advance the understanding of the transglycosylation mechanism of EndoSz-D234M, the *apo*- and *holo*-structures of Δ*E*ndoSz-D234M were determined, of which the high-resolution *holo*-structure of Δ*E*ndoSz-D234M was solved with a novel pH-jump method (Figure S6b). The complex structure of EndoSz-D234M/G2S2-oxazoline clearly shows that oxazoline sits in the oxa-hole. The holes are also found in the structures of EndoS and EndoS2, highlighting the importance of the oxa-hole. Combining the *apo*- and *holo*-structures of EndoSz-D234M and transglycosylation activity studies, the stepwise transglycosylation mechanism of EndoSz-D234M mediated by loop2 is revealed. The mutations D234M/E236A and D234M/W154G resulted in ∼97 and ∼36% decreased transglycosylation activities, respectively, compared to EndoSz-D234M, agreeing with our proposed transglycosylation mechanism. The hydrogen bond between Trp154 on loop2 and O4 of Man (−2) plays an important role in transglycosylation activities. The oxa-hole can accommodate oxazoline to perform the further transglycosylation reaction. Inside the oxa-hole, the H-bond network involved with Met234, water, oxazoline nitrogen, and Glu236 plays an important role in the transglycosylation activity. Moreover, the weak hydrogen bond between M234 and the oxazoline nitrogen is a good starting point for developing the new glycosynthase variant for better antibody-specific transglycosylation activity.

METHODS

Materials

The monoclonal anti-Globo-H antibody (OBI-888) and the anti-SSEA4 antibody (OBI-898) were produced as per our previous procedures disclosed in the Patent Cooperation Treaty (PCT) patents WO2017062792A1 and WO2017172990A1, respectively. The commercial antibodies Herceptin (transtuzumab), Perjeta (pertuzumab), Erbitux (Cetuximab), Rituxan (rituximab), Vectibix (panitumumab), Humira (Adalimumab), Keytruda (pembrolizumab), and Bavencio (Avelumab) were purchased from vendor companies. Biantennary glycan, sialylated complex-type *N*-glycan (NSCT), was purchased from Tokyo Chemical Industry Co., Ltd. (Tokyo, Japan, D4065). NSCT-oxazoline (G2S2-oxazoline), other glycans (M3, G0, and G2), and *Bf*-α-fucosidase were produced based on previous works.[27−29]

Molecular Cloning, Overexpression, and Purification of EndoSd, EndoSz, and Mutants

The genes of EndoSd and EndoSz from *S. dysgalactiae subsp. Dysgalactiae* (ANI26082.1) and *S. equi subsp. Zooepidemicus Sz105* (KIS14581.1) were used for this study. The N-terminal signal peptides were deleted in both enzymes. To enhance the transglycosylation activity, we aligned the protein sequences of EndoSd, EndoSz, and EndoS2-D184M[27] and found D232 and D234 at the relative positions as key catalytic residues for EndoSd and EndoSz, respectively. We then mutated the relative position Asp to Met. Therefore, the genes encoding amino acids 20−1067 of EndoSd-D232M and 20−1011 of EndoSz-D234M were synthesized and subcloned into pGEX-4T-1 with 5′-*Bam*HI and 3′-XhoI restriction sites. For purification purposes, we inserted an additional six histidines at the C-terminal of EndoSd-D232M and EndoSz-D234M for the Ni-NTA affinity column. Other mutants used in this investigation were generated by site-directed mutagenesis. Related primers were designed based on the mutated sites. Taking EndoSd-D232M and EndoSz-D234M as template vectors, the mutated vectors were amplified by the Pfu DNA polymerase (Protech). The template vectors (methylated DNA) were then digested with DpnI (Promega) at 37 °C for 2 h. The mutated vectors were transformed into DH5α competent cells for selection. All mutants were confirmed by DNA sequencing.

All vectors were transformed into BL21 (DE3) and cultured at 37 °C in a TB medium containing the ampicillin antibiotic (50 μg/mL). The proteins were induced by isopropyl-β-D-thiogalactopyranoside (IPTG, 0.2 mM), while the cell density OD_{600} reached 0.6. After 5 h, the cells were harvested at 25 °C with centrifugation (BACKMAN/JLA-8.1, 9000 g) for 15 min. The cell pellet was suspended (100 mL buffer/1 L cell pellet) with a wash buffer containing MOPS (50 mM, pH 7.0), NaCl (300 mM), and imidazole (10 mM) with a homogenizer (NanoLyzer N-10) to break the cells. After

https://doi.org/10.1021/jacsau.4c00004
JACS Au 2024, 4, 2130−2150

centrifugation (12 000*g*, BACKMAN/JA-10) at 4 °C for 60 min, the pellet was discarded, and the supernatant was then mixed with Ni-NTA resin (Roche) and gently rocked at 4 °C overnight for complete protein binding. The resin was loaded onto the open column and, subsequently, the nonbound protein was washed with a wash buffer until the concentration of the nonbound protein was less than 1 mg/mL (defined by the Bradford assay, Thermo). The bound protein was eluted with an elution buffer containing MOPS (50 mM, pH 7.0), NaCl (300 mM), and imidazole (250 mM). The eluted fraction was dialyzed against a storage buffer containing MOPS (50 Mm, pH 6.7) and concentrated with TFF (Millipore lab scale) by a 30 kDa cutoff cassette. The final samples were assayed by 4−12% gradient SDS-PAGE and Bradford to examine the correct molecular masses and concentrations, respectively.

Deglycosylation of mAbs

The *N*-glycans of mAbs (10 mg) were digested by incubating with wild-type EndoSz (10 μg) and *Bf*-α-fucosidase (10 mg) in the Tris-HCl buffer (pH 7.4) at 30 °C for 16 h to generate mAbs-GlcNAc. Fucosylated mAb-GlcNAc (mAbs-GlcNAc-F) were produced by only wild-type EndoSz in a similar condition with a 4-h incubation time.

Transglycosylation of Glycans to mAb-GlcNAc and mAb-GlcNAc-F

In general procedures, mAb-GlcNAc/mAb-GlucNAc-F (5 mg) was incubated with glycan-oxa with molar ratios of 1:20 and 1:150 (mAb-GlcNAc/G2S2-oxazoline), respectively. The mixtures of 1:20 and 1:150 were reacted with EndoSz-D234M (167 μg) and EndoSd-D232M (1002 μg), respectively, in a MOPS buffer (50 mM, pH 6.7, final volume 500 μL) at 30 °C for 20 min. There were some slight modifications according to experimental purposes and designs (see Result and Discussion). HLPC was employed to monitor the transglycosylation efficiency.

Purification of Deglycosylated and Homogeneous mAbs

The reaction mixture was applied to a HiTrap Protein-A HP (5 mL, GE) prepacked column, which was pre-equilibrated with the PBS buffer. The nonbound contaminations were washed off by a two-step pH gradient with PBS (pH 7.4) buffer and glycine-HCl (pH 5.0) buffer, with five times the column volume in each step. Sodium citrate (pH 3.0) was employed to elute the bound antibody. The eluted fractions were immediately neutralized with Tris-HCl buffer (1 M, pH 9.0) to pH 7.4 and dialyzed against the storage buffer containing MOPS (50 mM, pH 6.7) for mAb-GlcNAc(F) and histidine (5 mM) and NaCl (150 mM) for mAb-G2S2, with a 30 kDa cutoff dialysis cassette (Thermo) at 4 °C overnight. All samples were concentrated with the Amicon centrifugation membrane (30 kDa cutoff, Millipore) and stored at 4 °C [mAb-GlcNAc(F)] or −80 °C [mAb-G2S2(F)].

Enzymatic Transglycosylation Assay by HPLC

The glycosynthase activity was analyzed by HPLC (Waters e2695) using the UPLC Glycoprotein Amide column (2.1 mm × 150 mm, Waters) under two different buffers: buffer A, ddH_2O/0.3% v/v HFIP (1,1,1,3,3,3-hexafluoro-2-propanol), 0.1% v/v TFA (trifluoroacetic acid); buffer B, ACN, 0.3% v/v HFIP, 0.1% v/v TFA with gradient elution. The gradient program was set from 85% B at a flow rate of 0.2 mL/min for 1 min, followed by a linear decrease to 67% B at a flow rate of 0.2 μL/min over 0.5 min and the gradient was continuously decreased to 61.4% B over 16 min. At this point, 61.4% B at a flow rate of 0.2 mL/min was maintained for 3 min and then the gradient was increased to 85% B in 1 min and kept at 85% B at a flow rate of 0.2 mL/min for 9 min.

ADCC Assay

The ADCC activity was analyzed by the ADCC reporter bioassay complete kit (Promega, G7015) using luciferase reporter cells. The related cell lines MCF7W (OBI-888), SKBR-3 (Herceptin, Perjeta), BxPC3 (Erbitux), and Raji (Rituxan) were selected for analysis. All cell lines shared the same procedures. Target cells were seeded on a 96-well cell culture plate and incubated at 37 °C in a humidified 5% CO_2 incubator overnight. The culture medium was replaced with a serial dilution of homogeneous antibodies and the corresponding antibody standard in triplicate. In each well, ADCC bioassay effector cells were added. The ratio of effector cells to target cells was 3:1. We performed induction for 6 h and then added the Bio-Glo luciferase assay buffer. After 15 min, luminescence (RLU, relative light unit) was determined using a microplate reader (SpectraMax L, Molecular Devices, Sunnyvale, CA). The fold change of luminescence induction was calculated by the ratio of relative light unit (RLU) (induced) to RLU (no antibody control). EC_{50} was determined by plotting x (concentration in μg/mL) − y (induction of fold change), and data was fit in a 4PL nonlinear regression model by *Prism* 6 software. The relative potency was estimated with a parallel-line analysis using Gen5 Microplate Reader and Imager software (BioTek Instruments).

Overexpression and Purification of Truncated EndoSz for Crystallization

The plasmid of PET_4T_1 bearing the gene of the truncated Δ*E*ndoSz-D234M (a.a. 99−974) with six histidine residues at the C-terminus was designed and provided by the OBI company. The plasmid was transformed into BL21 cells. The cells carrying the target plasmid were cultured in LB (3 mL) with ampicillin (100 μg/mL) using vigorous shaking at 37 °C overnight. The cultured cells were further inoculated at LB (1 L) by adding ampicillin (2 mL, 100 μg/mL). The 1 L cells were cultivated with vigorous shaking at 37 °C, and the optical density (OD) was monitored at a wavelength of 595 nm with a spectrometer (Varian) during cell cultivation. After the OD reached 0.4−0.6 in ∼3 h, isopropyl β-D-1 thiogalactopyranoside (IPTG, 0.4 mM) was added to the cultivated cells. The over-expression-induced cells were cultured with gentle shaking at 18 °C for 18 h. The overexpressed cells were harvested by centrifugation at 9000*g* for 25 min (Kubota). The harvested cells were disrupted using ultrasonication, and cell debris was removed with centrifugation at 10 000*g*. The supernatant from disrupted cells was applied to Ni-NTA chromatography with an equilibrant buffer (20 mM Tris, pH 7.5, 300 mM NaCl). The gradient imidazole (30, 50, 100, 300, and 500 mM) was utilized to elute the proteins bound on the Ni-NTA resin. Each fraction was collected and analyzed by SDS-PAGE. The elution fractions with imidazole of 100, 300, and 500 mM were combined and dialyzed against a buffer (20 mM Tris, pH 7.5, 300 mM NaCl). The dialyzed Δ*E*ndoSz-D234M was reacted with thrombin to remove the tag of glutathione S-transferase (GST tag) at 4 °C for 18 h. The cleaved proteins were injected into the Ni-NTA column, and purification was conducted using an equilibrant buffer (20 mM Tris, pH 7.5, 300 mM NaCl), a washing buffer (20 mM Tris, pH 7.5, 50 mM NaCl), and an elution buffer (20 mM Tris, pH 7.5, 500 mM NaCl). The eluted Δ*E*ndoSz-D234M was dialyzed against a buffer (20 mM Tris, pH 7.5, 100 mM NaCl) for 18 h. Finally, size-exclusion chromatography (SEC) with the buffer (20 mM Tris pH 7.5, 100 mM NaCl) was performed. The eluted Δ*E*ndoSz-D234M was concentrated to 12 mg/mL using Amicon with a M_w cutoff of 50 kDa and subsequently applied to the crystallization experiments. The over-expression and purification procedures of the full-length EndoSz-D234M were the same as those of Δ*E*ndoSz-D234M. Both the truncated and full-length EndoSz-D234M showed monomer forms in SEC.

Crystallization and Data Collection of Truncated *apo*-EndoSz-D234M

The purified full-length and Δ*E*ndoSz-D234M were both applied to the crystallization experiment with the hanging-drop vapor-diffusion method. No crystal of the full-length EndoSz could be observed, which might be due to the highly flexible N- or C-terminus. In contrast, two crystal forms of Δ*E*ndoSz were obtained with two different crystallization conditions. The laminar-shaped crystal was crystallized with the condition containing sodium citrate (0.1 mM, pH 5.4) and ammonium sulfate (2.2 M), whereas the rice-shaped crystal was obtained from the condition with sodium HEPES (0.1 M, pH 7.5) and sodium citrate tribasic (1.4 M). These crystals were validated with X-rays, and the data were collected using the wavelength of 1 Å at the TPS 05A1 beamline of NSRRC in Taiwan. The laminar-shaped crystal belonged to the space group $P2_1$, whereas the rice-shaped

https://doi.org/10.1021/jacsau.4c00004
JACS Au 2024, 4, 2130−2150

Table 3. Data Collection and Structural Refinement Statistics[a]

crystal form (PDB entry)	unbound ($P2_1$) (8W4I)	unbound ($P2_12_12_1$) (8W4G)	complex ($P2_1$) (8W4N)	complex ($P2_12_12_1$) (8X8G)
resolution range	27.76−2.91 (3.01−2.91)	42.57−2.15 (2.23−2.15)	28.33−3.10 (3.21−3.10)	45.28−2.27 (2.35−2.27)
space group	$P2_1$	$P2_12_12_1$	$P2_1$	$P2_12_12_1$
unit cell (Å/°)	51.41, 101.72, 129.24 / 90.37	50.95, 101.21, 234.58	51.59, 101.69, 129.80 / 90.72	50.65, 101.06, 232.60
unique reflections	29 373 (2912)	66 610 (6627)	24 061 (2397)	56 112 (5570)
completeness (%)	99.53 (99.01)	99.12 (99.94)	98.23 (98.20)	99.58 (100.00)
mean I/sigma (I)	8.4 (1.5)	6.8 (1.5)	5.0 (1.2)	6.3 (2.0)
multiplicity	2.0 (2.0)	3.2 (3.2)	1.8 (1.8)	3.2 (3.2)
$CC_{1/2}$ (%)	99.1 (59.2)	99.5 (68.3)	96.8 (54.0)	99.5 (61.0)
reflections used in refinement	29 364 (2912)	66 558 (6626)	24 061 (2397)	56 112 (5570)
reflections used for R_{free}	2002 (204)	3140 (340)	1987 (195)	2846 (293)
R_{work} (%)	23.12 (31.97)	21.51 (30.33)	22.96 (34.52)	20.79 (26.31)
R_{free} (%)	27.08 (36.50)	25.09 (32.27)	27.50 (40.47)	24.83 (29.11)
number of non-hydrogen atoms	6903	7345	7021	7334
macromolecules	6902	6902	6,902	6902
ligands	1	1	119	138
solvent	0	442	0	294
protein residues	876	876	876	876
RMS (bonds Å)	0.007	0.009	0.003	0.008
RMS (angles °)	1.08	1.08	0.72	1.02
ramachandran favored (%)	92.22	92.68	95.42	95.08
ramachandran allowed (%)	7.21	7.21	4.23	4.92
ramachandran outliers (%)	0.57	0.13	0.34	0.00
rotamer outliers (%)	1.33	0.13	0.40	0.00
clashscore	9.86	11.02	5.48	6.99
average B-factor (Å^2)	69.95	57.36	79.79	56.25
macromolecules	69.95	57.81	78.82	55.97
ligands	90.68	83.73	118.46	84.42

[a]Values in parentheses are for the highest-resolution shell. $CC_{1/2}$ is the percentage of correlation between intensities of random half-data sets.

crystal belonged to the space group $P2_12_12_1$. The details of data statistics of both crystal forms are summarized in Table 3.

Soaking Experiments (pH Jump) with G2S2-Oxazoline and Data Collection of the EndoSz-D234M Complex

Because of the higher resolution, crystals of the space group $P2_12_12_1$ were first applied to the soaking experiment with the substrate G2S2-oxazoline. The corresponding crystallization condition of $P2_12_12_1$ crystals was applied to the cocrystallization experiment with the substrate sugar of different ratios. The crystals grown from the cocrystallization experiment were applied in the X-ray data collection or the further soaking experiment (cocrystallization plus soaking method). More than 100 X-ray data sets of these crystals were collected at the beamlines TPS 05A1 of NSRRC in Taiwan and BL44XU of SPring-8 in Japan, but no extra electron density for the substrate sugar was observed with these data sets. Finally, the crystals of space group $P2_12_12_1$ were transferred and soaked overnight in the acid solution containing sodium citrate (0.1 mM, pH 5.4) and ammonium sulfate (2.0 M). The crystals were then further soaked with 0.5 mM G2S2-oxazoline for 6−10 min. The crystals were then picked and transferred into a solution (0.1 mM sodium citrate, pH 5.4, 2.0 M ammonium sulfate) containing additional glycerol (20%) as a cryo-protectant and then were fast-frozen in LN_2. These frozen crystals were applied to data collection using wavelengths of 1 and 0.9 Å at the beamlines TPS 05A1 in NSRRC (Hsinchu, Taiwan) and BL44XU in SPring-8 (Hyogo, Japan), respectively. Finally, the data of the complex crystal with G2S2-oxazoline was successfully collected at the highest resolution 2.2 Å.

Structure Determination of *apo*-EndoSz-D234M and Its Complex with G2S2-Oxazoline

The initial phase of *apo*-Δ*E*ndoSz-D234M was determined with the molecular replacement method with a search model of EndoS (PDB entry 4NUY) using the program *Phaser* in *Phenix*.[58] The iterative model building and refinement using *Coot*[59] and *Phenix* were conducted. The structure determination of Δ*E*ndoSz-D234M in complex with G2S2-oxazoline was carried out with the molecular replacement method with a search model of determined *apo*-Δ*E*ndoSz-D234M using *Molrep*[60] in the *CCP4* suite.[61] The sugar moieties were built one by one, and the iterative refinement was performed based on electron density maps with coefficients $F_o - F_c$ and $2F_o - F_c$. Finally, all 10 sugar moieties of the G2S2-oxazoline were built. The structures of the *apo*-form and the complex form were validated using *Molprobity*.[62] The statistics of structure refinement are given in Table 3. The interactions between EndoSz-D234M and G2S2-oxazoline were delineated clearly. All structural graphics and analyses were conducted by *PyMol*[63] and the UCSF Chimera package.[64]

Crystallization, Data Collection, and Structure Determination of Closed and Open Forms of IgG-Fc in the Presence of EndoSz-D234M

The purified Δ*E*ndoSz-D234M (25 mg/mL) was mixed with the purified IgG-Fc (29 mg/mL) at a molar ratio of 1:1 and then incubated on ice for 4 h. The mixture was applied in the crystallization experiments using the hanging-drop vapor-diffusion method. The rice-shaped crystals of IgG-Fc in the closed form were grown in the crystallization condition (100 mM MES, pH 6, 200 mM zinc acetate, and 10% PEG8000) at 18 °C in 6 days, whereas the cuboid crystals of IgG-Fc in the open form were grown in the crystallization condition (100 mM MES, pH 6.5, 200 mM zinc acetate, and 10% PEG8000) at 18 °C in 18 months. The X-ray diffraction data sets of IgG-Fc crystals of both closed and open forms were, respectively, collected at the beamlines TPS 05A1 of NSRRC in Taiwan and BL44XU of SPring-8 in Japan. The structures of IgG-Fc in closed and open forms were determined with the molecular replacement method with the search models dimeric and monomeric IgG-Fc (PDB entries: 1H3Y), respectively. Both refined structures were validated using *Molprobity*.[62]

https://doi.org/10.1021/jacsau.4c00004
JACS Au 2024, 4, 2130−2150

The statistics of X-ray data and structure refinement are given in Table S3.

Molecular Docking of EndoSz-D234M toward the Open Form of IgG-Fc

The determined structure of *holo*-ΔEndoSz-D234M (PDB entry 8X8G) was docked onto the open form of IgG-Fc (PDB entry 8W4M) according to the CryoEM complex structure of EndoS/IgG-Fc (PDB entry 8A64). The sugar moieties (−1 to −10) on the open form of IgG-Fc were removed and followed by the molecular docking of ΔEndoSz-D234M toward the modified open form of IgG-Fc, with only NAG(+1), using the *HADDOCK* (High Ambiguity Driven protein−protein Docking) software.[65,66] The simulated complex structure of ΔEndoSz-D234M with IgG-Fc was utilized for further structural analysis.

■ ASSOCIATED CONTENT

Data Availability Statement

The main data supporting the findings of this study are available within the article and its Supporting Information. The determined structures and corresponding structure factors have been deposited to the Protein Data Bank under accession entries 8W4I (*apo*-ΔEndoSz-D234M, $P2_1$), 8W4G (*apo*-ΔEndoSz-D234M, $P2_12_12_1$), 8W4N (*holo*-ΔEndoSz-D234M, $P2_1$), 8X8G (*holo*-ΔEndoSz-D234M, $P2_12_12_1$), 8W4L (closed form of IgG-Fc), and 8W4M (open form of IgG-Fc).

Supporting Information

The Supporting Information is available free of charge at https://pubs.acs.org/doi/10.1021/jacsau.4c00004.

Glycoform release; glycan analyses; solution state; CBM comparisons; pH-jump experiments; bound biantennary glycan; substrate selectivity; key residue interactions; mobile conformation; closed/open forms; modeled complexes; H-bond networks; time course study; transglycosylation activities; and crystal data (PDF)

■ AUTHOR INFORMATION

Corresponding Authors

Yih-Huang Hsieh − *OBI Pharma, Inc., Taipei City 115, Taiwan*; Email: edwardhsieh@obipharma.com

Chun-Jung Chen − *Life Science Group, Scientific Research Division, National Synchrotron Radiation Research Center, Hsinchu 300092, Taiwan; Institute of Biotechnology and industry Science, and University Center for Bioscience and Biotechnology, National Cheng Kung University, Tainan 701, Taiwan; Department of Physics, National Tsing Hua University, Hsinchu 300044, Taiwan; Department of Biological Science and Technology, National Yang Ming Chiao Tung University, Hsinchu 300093, Taiwan;* orcid.org/0000-0002-5157-4288; Email: cjchen@nsrrc.org.tw

Authors

Yin-Cheng Hsieh − *OBI Pharma, Inc., Taipei City 115, Taiwan*

Hong-Hsiang Guan − *Life Science Group, Scientific Research Division, National Synchrotron Radiation Research Center, Hsinchu 300092, Taiwan*

Chien-Chih Lin − *Life Science Group, Scientific Research Division, National Synchrotron Radiation Research Center, Hsinchu 300092, Taiwan*

Teng-Yi Huang − *OBI Pharma, Inc., Taipei City 115, Taiwan*

Phimonphan Chuankhayan − *Life Science Group, Scientific Research Division, National Synchrotron Radiation Research Center, Hsinchu 300092, Taiwan*

Nai-Chi Chen − *Life Science Group, Scientific Research Division, National Synchrotron Radiation Research Center, Hsinchu 300092, Taiwan*

Nan-Hsuan Wang − *OBI Pharma, Inc., Taipei City 115, Taiwan*

Pu-Ling Hu − *OBI Pharma, Inc., Taipei City 115, Taiwan*

Yi-Chien Tsai − *OBI Pharma, Inc., Taipei City 115, Taiwan*

Yen-Chieh Huang − *Life Science Group, Scientific Research Division, National Synchrotron Radiation Research Center, Hsinchu 300092, Taiwan*

Masato Yoshimura − *Life Science Group, Scientific Research Division, National Synchrotron Radiation Research Center, Hsinchu 300092, Taiwan*

Pei-Ju Lin − *Life Science Group, Scientific Research Division, National Synchrotron Radiation Research Center, Hsinchu 300092, Taiwan*

Complete contact information is available at: https://pubs.acs.org/10.1021/jacsau.4c00004

Author Contributions

#Y.-C.H. and H.-H.G. contributed equally to this work; C.-J.C and Y.-H.H. initiated the project; Y.-C.H., T.-Y.H., N.-H.W., P.-L.H., and Y.-C.T. performed functional studies; H.-H.G. and C.-C.L. performed X-ray data collection and structure determination; Y.-C.H., H.-H.G. C.-C.L., P.C., N.-C.C., M.Y., P.-J.L., and C.-J.C. analyzed the data; and Y.-C.H., H.-H.G., and C.-J.C. designed the study and wrote the paper. CRediT: **Yin-Cheng Hsieh** data curation, formal analysis, investigation, writing-original draft, writing-review & editing; **Hong-Hsiang Guan** data curation, formal analysis, investigation, validation, writing-original draft, writing-review & editing; **Chien-Chih Lin** data curation, formal analysis, validation; **Teng-Yi Huang** data curation, formal analysis; **Phimonphan Chuankhayan** formal analysis; **Nai-Chi Chen** formal analysis; **Nan-Hsuan Wang** data curation, formal analysis; **Pu-Ling Hu** formal analysis; **Yi-Chien Tsai** formal analysis; **Yen-Chieh Huang** formal analysis; **Masato Yoshimura** data curation, formal analysis; **Pei-Ju Lin** formal analysis; **Yih-Huang Hsieh** conceptualization, writing-original draft; **Chun-Jung Chen** conceptualization, formal analysis, funding acquisition, investigation, methodology, project administration, resources, software, supervision, validation, writing-original draft, writing-review & editing.

Funding

This work was supported by the National Science and Technology Council (NSTC) grants 105-2311-B-213-001-MY3, 107-2923-B-213-001-MY3, 108-2311-B-213-001-MY3, 111-2311-B-213-001, and 112-2311-B-213-001; OBI Pharma Inc. grants 106C-OBI, 108C04, and 109C04; and NSRRC grants 1112315AR1, 11123LAB02, 1122315AR1, and 11223LAB02 to C.-J. Chen.

Notes

The authors declare no competing financial interest.

■ ACKNOWLEDGMENTS

The authors are indebted to the colleagues and staff at beamlines TPS 05A1, TPS 07A1, and TLS BL15A1 of the National Synchrotron Radiation Research Center (NSRRC) at

Hsinchu, Taiwan, and at the BL44XU of SPring-8 with proposal numbers ICR-21-05, ICR-22-05, and ICR-23-05 at Hyogo, Japan, for assistance with the data collection. This research was carried out in part at the NSRRC-NCKU Protein Crystallography Laboratory. The authors are grateful to the University Center for Bioscience and Biotechnology, National Cheng Kung University, for the support.

■ ABBREVIATIONS

mAbs, monoclonal antibodies; ENGase, endo-β-*N*-acetylglucosaminidase; ADCC, antibody-dependent cellular cytotoxicity; CDC, complement-dependent cytotoxicity; Oxa-hole, oxazoline-hole

■ REFERENCES

(1) Ecker, D. M.; Jones, S. D.; Levine, H. L. The therapeutic monoclonal antibody market. *MAbs* **2015**, *7* (1), 9.
(2) Lu, R.-M.; Hwang, Y.-C.; Liu, I. J.; Lee, C.-C.; Tsai, H.-Z.; Li, H.-J.; Wu, H.-C. Development of therapeutic antibodies for the treatment of diseases. *J. Biomed. Sci.* **2020**, *27*, 1.
(3) Urquhart, L. Top companies and drugs by sales in 2021. *Nat. Rev. Drug Discovery* **2022**, *21* (4), 251.
(4) Adams, G. P.; Weiner, L. M. Monoclonal antibody therapy of cancer. *Nat. Biotechnol.* **2005**, *23* (9), 1147.
(5) Aggarwal, S. What's fueling the biotech engine. *Nat. Biotechnol.* **2012**, *30*, 1191.
(6) Aggarwal, S. A survey of breakthrough therapy designations. *Nat. Biotechnol.* **2014**, *32* (4), 323.
(7) Jefferis, R. Glycosylation as a strategy to improve antibody-based therapeutics. *Nat. Rev. Drug Discovery* **2009**, *8* (3), 226.
(8) Bournazos, S.; Corti, D.; Virgin, H. W.; Ravetch, J. V. Fc-optimized antibodies elicit CD8 immunity to viral respiratory infection. *Nature* **2020**, *588* (7838), 485.
(9) Shivatare, S. S.; Shivatare, V. S.; Wong, C.-H. Glycoconjugates: synthesis, functional studies, and therapeutic developments. *Chem. Rev.* **2022**, *122* (20), 15603.
(10) Shivatare, V. S.; Chuang, P.-K.; Tseng, T.-H.; Zeng, Y.-F.; Huang, H.-W.; Veeranjaneyulu, G.; Wu, H.-C.; Wong, C.-H. Study on antibody Fc-glycosylation for optimal effector functions. *Chem. Commun.* **2023**, *59* (37), 5555.
(11) Ferrara, C.; Grau, S.; Jager, C.; Sondermann, P.; Brunker, P.; Waldhauer, I.; Hennig, M.; Ruf, A.; Rufer, A. C.; Stihle, M.; et al. Unique carbohydrate-carbohydrate interactions are required for high affinity binding between Fc RIII and antibodies lacking core fucose. *Proc. Natl. Acad. Sci. U.S.A.* **2011**, *108* (31), 12669.
(12) Kurogochi, M.; Mori, M.; Osumi, K.; Tojino, M.; Sugawara, S. I.; Takashima, S.; Hirose, Y.; Tsukimura, W.; Mizuno, M.; et al. Glycoengineered monoclonal antibodies with homogeneous glycan (M3, G0, G2, and A2) using a chemoenzymatic approach have different affinities for FcγRIIIa and variable antibody-dependent cellular cytotoxicity activities. *PLoS One* **2015**, *10* (7), No. e0132848.
(13) Yamane-Ohnuki, N.; Satoh, M. Production of therapeutic antibodies with controlled fucosylation. *MAbs* **2009**, *1*, 230.
(14) Yamane-Ohnuki, N.; Kinoshita, S.; Inoue-Urakubo, M.; Kusunoki, M.; Iida, S.; Nakano, R.; Wakitani, M.; Niwa, R.; Sakurada, M.; Uchida, K.; et al. Establishment of FUT8 knockout Chinese hamster ovary cells: An ideal host cell line for producing completely defucosylated antibodies with enhanced antibody-dependent cellular cytotoxicity. *Biotechnol. Bioeng.* **2004**, *87* (5), 614.
(15) Umaña, P.; Jean-Mairet, J.; Moudry, R.; Amstutz, H.; Bailey, J. E. Engineered glycoforms of an antineuroblastoma IgG1 with optimized antibody-dependent cellular cytotoxic activity. *Nat. Biotechnol.* **1999**, *17*, 176.
(16) Hogenkamp, D. G.; Arakane, Y.; Kramer, K. J.; Muthukrishnan, S.; Beeman, R. W. Characterization and expression of the β-*N*-acetylhexosaminidase gene family of Tribolium castaneum. *Insect Biochem. Mol. Biol.* **2008**, *38* (4), 478.
(17) Fairbanks, A. J. The ENGases: versatile biocatalysts for the production of homogeneous N-linked glycopeptides and glycoproteins. *Chem. Soc. Rev.* **2017**, *46* (16), 5128.
(18) Maley, F.; B, T. R.; Tarentino, A. L.; Plummer, T. H., Jr. Characterization of glycoproteins and their associated oligosaccharides through the use of endoglycosidases. *Anal. Biochem.* **1989**, *180*, 195.
(19) Li, B.; Song, H.; Hauser, S.; Wang, L. X. A Highly efficient chemoenzymatic approach toward glycoprotein synthesis. *Org. Lett.* **2006**, *8*, 3081.
(20) Wang, L. X. Chemoenzymatic synthesis of glycopeptides and glycoproteins through endoglycosidase-catalyzed transglycosylation. *Carbohydr. Res.* **2008**, *343* (10−11), 1509.
(21) Rising, T. W. D. F.; Claridge, T. D.; Moir, J. W.; Fairbanks, A. J. Endohexosaminidase M: exploring and exploiting enzyme substrate specificity. *ChemBioChem* **2006**, *7* (8), 1177.
(22) Fairbanks, A. J. Chemoenzymatic synthesis of glycoproteins. *Curr. Opin. Chem. Biol.* **2019**, *53*, 9.
(23) Jefferis, R. Glycosylation of recombinant antibody therapeutics. *Biotechnol. Prog.* **2005**, *21*, 11.
(24) Liu, L. Antibody glycosylation and its impact on the pharmacokinetics and pharmacodynamics of monoclonal antibodies and Fc-fusion proteins. *J. Pharm. Sci.* **2015**, *104* (6), 1866.
(25) Collin, M.; Olsén, A. EndoS, a novel secreted protein from *Streptococcus pyogenes* with endoglycosidase activity on human IgG. *EMBO J.* **2001**, *20*, 3046.
(26) Sjögren, J.; Struwe, W. B.; Cosgrave, E. F. J.; Rudd, P. M.; Stervander, M.; Allhorn, M.; Hollands, A.; Nizet, V.; Collin, M. EndoS2 is a unique and conserved enzyme of serotype M49 group A Streptococcus that hydrolyses N-linked glycans on IgG and α1-acid glycoprotein. *Biochem. J.* **2013**, *455* (1), 107.
(27) Huang, W.; Giddens, J.; Fan, S.-Q.; Toonstra, C.; Wang, L.-X. Chemoenzymatic glycoengineering of intact IgG antibodies for gain of functions. *J. Am. Chem. Soc.* **2012**, *134* (29), 12308.
(28) Tai, T.; Yamashita, K.; Ogata-Arakawa, M.; Koide, N.; Muramatsu, T.; Iwashita, S.; Inoue, Y.; Kobata, A. Structural studies of two ovalbumin glycopeptides in relation to the endo-beta-N-acetylglucosaminidase specificity. *J. Biol. Chem.* **1975**, *250* (21), 8569.
(29) Tarentino, A. L.; Plummer, T. H., Jr.; Maley, F. The release of intact oligosaccharides from specific glycoproteins by endo-β-N-acetylglucosaminidase H. *J. Biol. Chem.* **1974**, *249*, 818.
(30) Kadowaki, S.; Yamamoto, K.; Fujisaki, M.; Izumi, K.; Tochikura, T.; Yokoyama, T. Purification and characterization of a novel fungal endo-β-N-acetylglucosaminidase acting on complex oligosaccharides of glycoproteins. *Agric. Biol. Chem.* **1990**, *54*, 97.
(31) Shadnezhad, A.; Naegeli, A.; Sjögren, J.; Adamczyk, B.; Leo, F.; Allhorn, M.; Karlsson, N. G.; Jensen, A.; Collin, M. EndoSd: an IgG glycan hydrolyzing enzyme in Streptococcus dysgalactiae subspecies dysgalactiae. *Future Microbiol.* **2016**, *11* (6), 721.
(32) Fan, S.-Q.; Huang, W.; Wang, L.-X. Remarkable transglycosylation activity of glycosynthase mutants of Endo-D, an Endo-β-*N*-acetylglucosaminidase from *Streptococcus pneumoniae*. *J. Biol. Chem.* **2012**, *287* (14), 11272.
(33) Umekawa, M.; Li, C.; Higashiyama, T.; Huang, W.; Ashida, H.; Yamamoto, K.; Wang, L. X. Efficient glycosynthase mutant derived from Mucor hiemalis endo-beta-N-acetylglucosaminidase capable of transferring oligosaccharide from both sugar oxazoline and natural *N*-glycan. *J. Biol. Chem.* **2010**, *285*, 511.
(34) Giddens, J. P.; Lomino, J. V.; Amin, M. N.; Wang, L.-X. Endo-F3 glycosynthase mutants enable chemoenzymatic synthesis of core-fucosylated triantennary complex type glycopeptides and glycoproteins. *J. Biol. Chem.* **2016**, *291* (17), 9356.
(35) Li, T.; Tong, X.; Yang, Q.; Giddens, J. P.; Wang, L.-X. Glycosynthase mutants of endoglycosidase S2 show potent transglycosylation activity and remarkably relaxed substrate specificity for antibody glycosylation remodeling. *J. Biol. Chem.* **2016**, *291* (32), 16508.
(36) Yin, J.; Li, L.; Shaw, N.; Li, Y.; Song, J. K.; Zhang, W.; Xia, C.; Zhang, R.; Joachimiak, A.; Zhang, H. C.; et al. Structural basis and

https://doi.org/10.1021/jacsau.4c00004
JACS Au 2024, 4, 2130−2150

catalytic mechanism for the dual functional endo-beta-N-acetylglucosaminidase A. *PLoS One* **2009**, *4* (3), No. e4658.
(37) Van Roey, P.; Rao, V.; Plummer, T. H. J.; Tarentino, A. L. Crystal Structure of endo-beta-N-acetylglucosaminidase F1, an alpha/beta-barrel enzyme. *Biochemistry* **1994**, *33*, 13989.
(38) Rao, V.; Cui, T.; Guan, C.; Van Roey, P. Mutations of endo-beta-N-acetylglucosamminidase H active site residues Asp130 and Glu132: activities and conformations. *Protein Sci.* **1999**, *8*, 2338.
(39) Stals, I.; Karkehabadi, S.; Kim, S.; Ward, M.; Van Landschoot, A.; Devreese, B.; Sandgren, M. High Resolution Crystal Structure of the Endo-N-Acetyl-β-D-Glucosaminidase Responsible for the Deglycosylation of *Hypocrea jecorina* Cellulases. *PLoS One* **2012**, *7* (7), No. e40854.
(40) Waddling, C. A.; Plummer, T. H. J.; Tarentino, A. L.; Van Roey, P. Structural basis for the substrate specificity of endo-beta-N-acetylglucosaminidase F3. *Biochemistry* **2000**, *39*, 7878.
(41) Trastoy, B.; Lomino, J. V.; Pierce, B. G.; Carter, L. G.; Gunther, S.; Giddens, J. P.; Snyder, G. A.; Weiss, T. M.; Weng, Z.; Wang, L. X.; Sundberg, E. J. Crystal structure of *Streptococcus pyogenes* EndoS, an immunomodulatory endoglycosidase specific for human IgG antibodies. *Proc. Natl. Acad. Sci. U.S.A.* **2014**, *111* (18), 6714.
(42) Trastoy, B.; Klontz, E.; Orwenyo, J.; Marina, A.; Wang, L.-X.; Sundberg, E. J.; Guerin, M. E. Structural basis for the recognition of complex-type *N*-glycans by Endoglycosidase S. *Nat. Commun.* **2018**, *9*, No. 1874.
(43) Klontz, E. H.; Trastoy, B.; Deredge, D.; Fields, J. K.; Li, C.; Orwenyo, J.; Marina, A.; Beadenkopf, R.; Gunther, S.; Flores, J.; et al. Molecular basis of broad spectrum *N*-glycan specificity and processing of therapeutic IgG monoclonal antibodies by endoglycosidase S2. *ACS Cent. Sci.* **2019**, *5* (3), 524.
(44) Sjögren, J.; Cosgrave, E. F.; Allhorn, M.; Nordgren, M.; Bjork, S.; Olsson, F.; Fredriksson, S.; Collin, M. EndoS and EndoS2 hydrolyze Fc-glycans on therapeutic antibodies with different glycoform selectivity and can be used for rapid quantification of high-mannose glycans. *Glycobiology* **2015**, *25* (10), 1053.
(45) Seki, H.; Huang, Y.; Arakawa, T.; Yamada, C.; Kinoshita, T.; Iwamoto, S.; Higuchi, Y.; Takegawa, K.; Fushinobu, S. Structural basis for the specific cleavage of core-fucosylated *N*-glycans by endo-beta-N-acetylglucosaminidase from the fungus Cordyceps militaris. *J. Biol. Chem.* **2019**, *294* (45), 17143.
(46) Trastoy, B.; Du, J. J.; Klontz, E. H.; Li, C.; Cifuente, J. O.; Wang, L. X.; Sundberg, E. J.; Guerin, M. E. Structural basis of mammalian high-mannose *N*-glycan processing by human gut Bacteroides. *Nat. Commun.* **2020**, *11* (1), No. 899.
(47) Shivatare, S. S.; Huang, L.-Y.; Zeng, Y.-F.; Liao, J.-Y.; You, T.-H.; Wang, S.-Y.; Cheng, T.; Chiu, C.-W.; Chao, P.; Chen, L.-T.; et al. Development of glycosynthases with broad glycan specificity for the efficient glyco-remodeling of antibodies. *Chem. Commun.* **2018**, *54* (48), 6161.
(48) Grzybowska, E. A. Calcium-binding proteins with disordered structure and their role in secretion, storage, and cellular signaling. *Biomolecules* **2018**, *8* (2), 42.
(49) Gallivan, J. P.; Gougherty, D. A. Cation-π interactions in structural biology. *Proc. Natl. Acad. Sci. U.S.A.* **1999**, *96*, 9459.
(50) Ahmed, A. A.; Giddens, J.; Pincetic, A.; Lomino, J. V.; Ravetch, J. V.; Wang, L. X.; Bjorkman, P. J. Structural characterization of anti-inflammatory immunoglobulin G Fc proteins. *J. Mol. Biol.* **2014**, *426* (18), 3166.
(51) Ramsland, P. A.; Farrugia, W.; Bradford, T. M.; Sardjono, C. T.; Esparon, S.; Trist, H. M.; Powell, M. S.; Tan, P. S.; Cendron, A. C.; Wines, B. D.; et al. Structural basis for FcγRIIa recognition of human IgG and formation of Inflammatory signaling complexes. *J. Immunol.* **2011**, *187* (6), 3208.
(52) Radaev, S.; Motyka, S.; Fridman, W.-H.; Sautes-Fridman, C.; Sun, P. D. The Structure of a Human Type III Fcγ Receptor in Complex with Fc. *J. Biol. Chem.* **2001**, *276* (19), 16469.
(53) Sondermann, P.; Huber, R.; Oosthuizen, V.; Jascob, U. The 3.2-Å crystal structure of the human IgG1 Fc fragment-FcgRIII complex. *Nature* **2000**, *406* (20), 267.
(54) Krapp, S.; Mimura, Y.; Jefferis, R.; Huber, R.; Sondermann, P. Structural analysis of human IgG-Fc glycoforms reveals a correlation between glycosylation and structural integrity. *J. Mol. Biol.* **2003**, *325* (5), 979.
(55) Frank, M.; Walker, R. C.; Lanzilotta, W. N.; Prestegard, J. H.; Barb, A. W. Immunoglobulin G1 Fc domain motions: Implications for Fc engineering. *J. Mol. Biol.* **2014**, *426* (8), 1799.
(56) Trastoy, B.; Du, J. J.; Cifuente, J. O.; Rudolph, L.; García-Alija, M.; Klontz, E. H.; Deredge, D.; Sultana, N.; Huynh, C. G.; Flowers, M. W.; et al. Mechanism of antibody-specific deglycosylation and immune evasion by *Streptococcal* IgG-specific endoglycosidases. *Nat. Commun.* **2023**, *14*, No. 1705.
(57) Wardman, J. F.; Bains, R. K.; Rahfeld, P.; Withers, S. G. Carbohydrate-active enzymes (CAZymes) in the gut microbiome. *Nat. Rev. Microbiol.* **2022**, *20* (9), 542.
(58) Adams, P. D.; Afonine, P. V.; Bunkoczi, G.; Chen, V. B.; Davis, I. W.; Echols, N.; Headd, J. J.; Hung, L. W.; Kapral, G. J.; Grosse-Kunstleve, R. W.; et al. *PHENIX*: a comprehensive Python-based system for macromolecular structure solution. *Acta Crystallogr., Sect. D: Biol. Crystallogr.* **2010**, *66* (Pt 2), 213.
(59) Emsley, P.; Cowtan, K. *Coot:* model-building tools for molecular graphics. *Acta Crystallogr., Sect. D: Biol. Crystallogr.* **2004**, *60* (12), 2126.
(60) Vagin, A.; Teplyakov, A. *Molrep*: an automated program for molecular replacement. *J. Appl. Crystallogr.* **1997**, *30*, 1022.
(61) Project, C. C. The CCP4 suite: programs for protein crystallography. *Acta Crystallogr., Sect. D: Biol. Crystallogr.* **1994**, *50* (Pt 5), 760.
(62) Chen, V. B.; Arendall, W. B., 3rd; Headd, J. J.; Keedy, D. A.; Immormino, R. M.; Kapral, G. J.; Murray, L. W.; Richardson, J. S.; Richardson, D. C. *MolProbity*: all-atom structure validation for macromolecular crystallography. *Acta Crystallogr., Sect. D: Biol. Crystallogr.* **2010**, *66* (Pt 1), 12.
(63) DeLano, W. L. *The Pymol Molecular Graphic System*; DaLano Scientific LLC: San Carlos, CA, 2009.
(64) Pettersen, E. F.; Goddard, T. D.; Huang, C. C.; Couch, G. S.; Greenblatt, D. M.; Meng, E. C.; Ferrin, T. E. UCSF Chimera–a visualization system for exploratory research and analysis. *J. Comput. Chem.* **2004**, *25* (13), 1605.
(65) De Vries, S. J.; Van Dijk, M.; Bonvin, A. M. The HADDOCK web server for data-driven biomolecular docking. *Nat. Protoc.* **2010**, *5* (5), 883.
(66) Van Zundert, G. C.; Rodrigues, J. P.; Trellet, M.; Schmitz, C.; Kastritis, P. L.; Karaca, E.; Melquiond, A. S.; van Dijk, M.; De Vries, S. J.; Bonvin, A. M. The HADDOCK2.2 web server: user-friendly integrative modeling of biomolecular complexes. *J. Mol. Biol.* **2016**, *428* (4), 720.

https://doi.org/10.1021/jacsau.4c00004
JACS Au 2024, 4, 2130−2150